© 2022. Published by The Company of Biologists Ltd | Development (2022) 149, dev199967. doi:10.1242/dev.199967

RESEARCH ARTICLE

PBAF chromatin remodeler complexes that mediate meiotic transitions in mouse

Rodrigo O. de Castro[1], Luciana Previato de Almeida[1], Agustin Carbajal[1], Irma Gryniuk[1] and Roberto J. Pezza[1,2,*]

ABSTRACT

Gametogenesis in mammals encompasses highly regulated developmental transitions. These are associated with changes in transcription that cause characteristic patterns of gene expression observed during distinct stages of gamete development, which include specific activities with critical meiotic functions. SWI/SNF chromatin remodelers are recognized regulators of gene transcription and DNA repair, but their composition and functions in meiosis are poorly understood. We have generated gamete-specific conditional knockout mice for ARID2, a specific regulatory subunit of PBAF, and have compared its phenotype with BRG1 knockouts, the catalytic subunit of PBAF/BAF complexes. While *Brg1*$^{\Delta/\Delta}$ knockout acts at an early stage of meiosis and causes cell arrest at pachynema, ARID2 activity is apparently required at the end of prophase I. Striking defects in spindle assembly and chromosome-spindle attachment observed in *Arid2*$^{\Delta/\Delta}$ knockouts are attributed to an increase in aurora B kinase, a master regulator of chromosome segregation, at centromeres. Further genetic and biochemical analyses suggest the formation of a canonical PBAF and a BRG1-independent complex containing ARID2 and PBRM1 as core components. The data support a model in which different PBAF complexes regulate different stages of meiosis and gametogenesis.

KEY WORDS: Mouse gametogenesis, SWI/SNF, PBAF, Meiosis, Testis development

INTRODUCTION

Spermatogenesis is the process by which diploid spermatogonia cells produce haploid mature gametes called spermatozoa. Spermatogenesis begins with primordial germ cell migration to the developing male gonad and division to produce an undifferentiated stem cell type of spermatogonia, which after maturation may commit to meiosis and is the precursor of primary spermatocytes. Primary spermatocytes undergo meiosis to halve their chromosome complement and yield a pair of secondary spermatocytes, which differentiate during spermiogenesis to produce haploid gametes (rounded spermatids, elongated spermatid and finally spermatozoa) (Cheng and Mruk, 2010). During prophase of meiosis I, homologous chromosomes pair, synapse and undergo recombination, which prepares them for segregation. Successful completion of these processes is required for the homologous chromosomes to mount the meiotic spindle as a pair.

Chromatin undergoes extensive remodeling during gametogenesis, leading to altered gene expression and chromosome organization, and ultimately controlling developmental transitions such as spermatogonia differentiation, meiotic commitment, and possibly stages of spermatogenesis and spermiogenesis. Chromatin remodeling complexes are a vast group of regulators with diverse functions in critical cellular processes such as transcription and DNA metabolism. These complexes use the energy of ATP-hydrolysis to physically disrupt histone-DNA contacts and move, destabilize, eject or restructure nucleosomes. One of these complexes is SWI/SNF, which exists in multiple forms with different subunit compositions, classified as one of three major complexes: BAF, PBAF and ncBAF. These complexes have considerable overlap in subunit composition with modular organization; however, they are defined by specific subunits: PBAF (PBRM1, BRD7 and ARID2); BAF (ARID1A and ARID1B); and ncBAF (BRD9) (de Castro et al., 2017; Mashtalir et al., 2018; Yan et al., 2005).

PBAF and BAF have been implicated in transcriptional regulation, development, cell differentiation, and, to a lesser extent, in DNA repair and genome stability (Hargreaves and Crabtree, 2011; Pulice and Kadoch, 2016; Centore et al., 2020). Ablation of BRG1, the catalytic subunit of PBAF/BAF, results in a profound defect in mouse spermatogenesis, which is associated with spermatocyte arrest at a pachytene-like stage, accumulation of unrepaired DNA and failure to complete chromosome synapsis. Previous reports have shown that germline-specific ablation of BRG1 results in gonadal developmental defect (Kim et al., 2012; Wang et al., 2012; Menon et al., 2019). Consistent with a role of BRG1 in double strand break (DSB) repair, knockout spermatocytes exhibit a prolonged γH2AX immunosignal (marker of DSBs) and an abnormally high level of irregularly distributed RAD51 foci. This is accompanied by incomplete synaptonemal complex formation and impaired synapsis (Kim et al., 2012). The PBAF-specific subunit ARID2 contains a defining N-terminal AT-rich DNA domain, common to the ARID protein family (Wilsker et al., 2005) and three additional domains: two DNA-binding domains (RFX domain; Emery et al., 1996) and a tandem C2H2 zinc-finger domain) and one protein-protein interaction domain. ARID2 is expressed in several tissues and is vital for embryonic development (He et al., 2014). Regarding the specific functions of ARID2, partial or complete deletion of this protein have revealed a role for ARID2 in the proliferation of embryonic cardiomyocytes (Xu et al., 2012), in embryonic death by E18.5 (Liu et al., 2018), and in osteogenic differentiation (Liu et al., 2018). An additional important aspect of ARID2 function is on the DNA damage response. Indeed, PBAF seems to be required to silence transcription in areas flanking DSBs and acts together with the PcG proteins to ensure efficient repair

[1]Cell Cycle and Cancer Biology Research Program, Oklahoma Medical Research Foundation, Oklahoma City, OK 73104, USA. [2]Department of Cell Biology, University of Oklahoma Health Science Center, Oklahoma City, OK 73104, USA.

*Author for correspondence (pezzar@omrf.org)

R.J.P., 0000-0003-0279-5516

Handling Editor: Haruhiko Koseki
Received 6 July 2021; Accepted 18 August 2022

Development (2022) 149, dev199967. doi:10.1242/dev.199967

(Kakarougkas et al., 2014). In another study, we demonstrated that ARID2 interacts with RAD51 and facilitates its recruitment to DSB sites, facilitating DNA repair via homologous recombination (de Castro et al., 2017). Not surprisingly, given the vast range of functions, *ARID2* mutations has been identified in many cancers, such as melanoma, urothelial cancer, gastric adenocarcinoma, non-small cell lung cancer and HCC (Mittal and Roberts, 2020), which agrees with a suggested role of ARID2 as a tumor suppressor (Helming et al., 2014; Manceau et al., 2013). Finally, in addition to cancers, some neurodevelopmental disorders have been linked to mutations in *ARID2* (Shang et al., 2015).

Although the results above suggest an important role for SWI/SNF in basic aspects of cell biology and during development in different tissues, several important questions remain unanswered. For example, given that BRG1 works as the catalytic subunit of both PBAF and BAF, its ablation affects both complexes. Thus, the common and individual contributions of PBAF and BAF during development are still not understood. This is particularly important in reproductive tissue and in meiotic cells, where the composition and the respective action mechanisms of complexes formed by the catalytic SWI/SNF unit BRG1 and regulatory units ARID2 and PBRM1 are not well understood. Another intriguing question is whether specific PBAF sub-complexes (i.e. those independent of BRG1) can efficiently perform specialized, but essential, cell or developmental functions. Indeed, it has been recently suggested that the heterogeneity in SWI/SNF subunits and/or the complex in higher eukaryotes allows the functional diversity required by the changing cellular needs and specialized functions of the differentiated cells (Ryme et al., 2009; Wang et al., 1996). These questions provided the impetus to examine the role of the PBAF-specific unit ARID2 in gamete development.

In this study, we explored the composition and functions of SWI/SNF complexes acting in mouse spermatogenesis. We observed that germ-specific ablation of ARID2 results in a phenotype distinctive from that observed for BRG1 deletion, and biochemical and genetic analysis show that ARID2 and PBRM1 form complexes independently of BRG1. We propose a model in which PBAF complexes containing BRG1 have a prominent function early in prophase I, and BRG1-independent complexes, such as those formed by ARID2 and PBRM1, regulate later developing gamete cellular functions, such as proper assembly and function of spindle and chromosome-spindle interactions.

RESULTS

Distinctive expression patterns for BRG1 and ARID2 during mouse spermatogenesis

We began exploring possible functions for components of the SWI/SNF chromatin remodeling complexes in male mouse gametogenesis by analyzing protein expression by immunostaining paraffin wax-embedded histological sections of testes (Fig. 1A). We used DAPI and SYCP3 staining for recognition of premeiotic and leptotene-zygotene, pachytene, diplotene stages of meiotic cell types and rounded spermatids. Specificity of primary antibodies against BRG1 and ARID2 was addressed by immunostaining paraffin wax-embedded cross-sections of BRG1 and ARID2 knockout testes (Figs S1 and S2). Antibodies to BRG1 showed prominent expression in spermatogonia and pachytene spermatocytes, and weaker staining in diplotene and in more advanced stages (e.g. round spermatids), as previously described (Kim et al., 2012; Wang et al., 2012). In contrast, analysis of ARID2 immunosignal revealed increased expression in meiotic cells in later stages of prophase I and in rounded spermatids (Fig. 1B). The differences in expression pattern between BRG1 and ARID2 initially suggested that these two SWI/SNF components may work at different stages of spermatogenesis.

Effect of ARID2 deletion in male reproductive tissues

To study the requisites of ARID2 in germ cell development, we generated ARID2 germ cell-specific conditional knockout mice. The mutation was created by inserting a LacZ-Neomycin cassette and a lox P site upstream of exon 4 and an additional loxP site downstream of exon 4 (Fig. 1C). A conditional (floxed, FL) allele was created by flipase recombinase expression (FRT) in mice carrying this allele. Subsequent Cre recombinase expression regulated by the promoters of the meiotic-specific genes *Ddx4* (Ddx4-Cre) or *Spo11* (Spo11-Cre) resulted in a germline-specific knockout mouse (Δ) (Fig. 1D,E). Ddx4-Cre (also known as Vasa) activity was directed to male and female germ cells starting at embryonic days 15-18. This allowed deletion of the *Arid2* gene as early as in primordial spermatogonia cells (prospermatogonia). In contrast, Spo11-Cre recombinase expression was detected in spermatocytes that have initiated meiosis, as early as postnatal day 10. The use of these Cre constructs allows: (1) evaluation of the earliest possible *Arid2* deletion phenotype (Ddx4-Cre); and (2) the bypass of a possible earlier requirement of *Arid2* and thus the evaluation of a later role in gametogenesis (e.g. meiosis or spermiogenesis) (Spo11-Cre).

Western blot analysis of whole testis of 2-month-old mice revealed that ARID2 was absent in Ddx4-$Arid2^{\Delta/\Delta}$ and Spo11-$Arid2^{\Delta/\Delta}$ mice, confirming depletion of ARID2 (Fig. 1E, Fig. S3A, B). No apparent changes in the expression of BRG1 were observed but there was a substantial reduction of PBRM1 expression in the knockouts. Reduction of PBRM1 in the chromatin may be caused by destabilization of PBRM1-containing complexes in the absence of ARID2, as we and others previously described in somatic cells (de Castro et al., 2017; Yan et al., 2005).

Compared with wild-type (0.108±0.014 g, n=8; n=26 testes, 13 mice) littermate testes in $Arid2^{\Delta/\Delta}$ adult mice were significantly smaller (Ddx4-$Arid2^{\Delta/\Delta}$ males: 0.044±0.004 g, n=6 testes, 3 mice, $P\leq0.0001$, two-tailed unpaired Student's t-test; Spo11-$Arid2^{\Delta/\Delta}$ males: 0.066±0.003 g, n=8 testes, 4 mice, $P\leq0.0001$). Ddx4-$Brg1^{\Delta/\Delta}$ knockout mice (0.035±0.004 g, n=6 testes, 5 mice) showed reduced testis size compared with wild type ($P\leq0.0001$) (Fig. 1F). Our results show that deletion of Arid2 affects testis development, suggesting that ARID2 has important functions during gametogenesis.

Histological and cellular analysis reveals defects in meiotic chromosome segregation in $Arid2^{\Delta/\Delta}$ mice testes

Analysis of paraffin wax-embedded testis sections stained with Hematoxylin and Eosin indicated that 2-month-old $Arid2^{\Delta/\Delta}$ males, generated using either Ddx4-Cre or Spo11-Cre, developed testicular hypoplasia with slight hyperplasia of interstitial cells and absent spermatozoa in epididymis (Fig. 2A and Fig. S4). Fertility analysis in males showed that Spo11-$Arid2^{\Delta/\Delta}$ mice were infertile, and no statistical difference was observed between Spo11-$Arid2^{Wt/\Delta}$ and $Arid2^{Wt/Wt}$ (Fig. S5A and Table S1). Hematoxylin and Eosin staining revealed that rounded spermatids and some elongated spermatids were apparently the most advanced spermatogenic cells in the $Arid2^{\Delta/\Delta}$ mice (Fig. 2G-I,L,M). A closer look revealed that chromosomes appeared to be normally condensed at metaphase I in $Arid2^{\Delta/\Delta}$ cells but, in contrast to wild type, in some cells the chromosomes failed to form normal metaphase plate figures and remained scattered throughout the nucleus with lagging chromosomes (wild type=2.5±0.024% of cells with

Development (2022) 149, dev199967. doi:10.1242/dev.199967

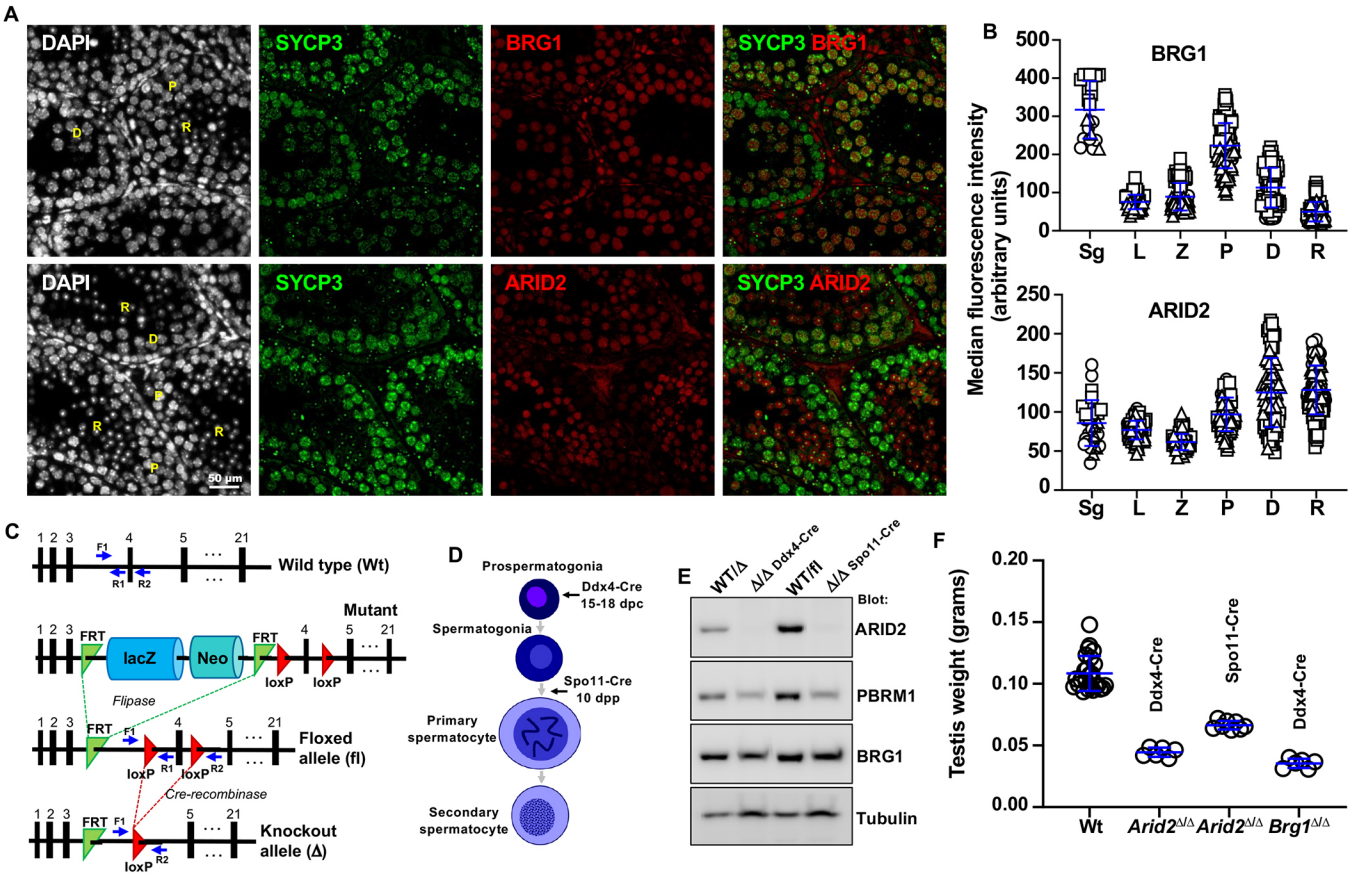

Fig. 1. Expression and function of BRG1 and ARID2 in mouse spermatogenesis. (A) Images show BRG1 and ARID2 immunostaining in paraffin wax-embedded sections of wild-type mice. P, pachytene; D, diplotene; R, rounded spermatid. (B) Immunosignal quantitation of BRG1 in spermatogonia (Sg) (arbitrary units, mean±s.d.) 317±76, *n*=24 cells; leptotene (L) 76±19, *n*=66; zygotene (Z) 90±36, *n*=106 total cell counted; pachytene (P) 223±59, *n*=168; diplotene (D) 113±52, *n*=101; rounded spermatids (R) 50±26, *n*=101) and of ARID2 (spermatogonia 86±29, *n*=29; leptotene 77±12, *n*=95; zygotene 62±11, *n*=74; pachytene 97±22, *n*=100; diplotene 124±44, *n*=77; rounded spermatid 128±31, *n*= 124) from images in A. Data were obtained in three different experiments from three different mice. (C) *Arid2* gene targeting design and subsequent deletion of exon 4. Gene location of F1, R1 and R2 oligonucleotides for PCR genotyping strategy used for detection of wild-type, floxed and delta mice are represented by blue arrows. (D) Diagram showing stages in gamete development and timing of expression for the Ddx4 and Spo11 promoters driving expression of the alternative Cre recombinases used in this study. (E) Western blots of 2-month-old testes of Arid2 knockout mice show no signal corresponding to the ARID2 protein compared with wild-type mice. Expression of PBRM1 and BRG1 in wild-type and *Arid2*$^{\Delta/\Delta}$ testis is also shown. Tubulin was used as loading standard. Results are shown for four mice: Ddx4-Arid2 control and knockout (left); and Spo11-Arid2 control and knockout (right). Quantitation of immunosignal can be found in Fig. S3C. (F) *Arid2* knockout mice (2-month old) have reduced testis size and testis weight compared with wild-type mice. *Brg1* knockout mice (2-month old) have reduced testis size and weight compared with Arid2 knockout and wild-type testes. Compared with wild-type (mean±s.d.) (0.108±0.014 g, *n*=8; *n*=26 testes, 13 mice) littermate testes in *Arid2*$^{\Delta/\Delta}$ adult mice are significantly smaller. Ddx4-*Arid2*$^{\Delta/\Delta}$ males (0.044±0.004 g, *n*=6 testes, 3 mice, $P \leq 0.0001$, *t*-test), Spo11-*Arid2*$^{\Delta/\Delta}$ males (0.066 g±0.003, *n*=8 testes, 4 mice, $P \leq 0.0001$, two-tailed unpaired Student's *t*-test). Ddx4-*Brg1*$^{\Delta/\Delta}$ knockout mice (0.035 g±0.004, *n*=6 testes, 5 mice) showed reduced testis size compared with wild type ($P \leq 0.0001$, two-tailed unpaired Student's *t*-test).

lagging chromosomes, *n*=122; Ddx4-*Arid2*$^{\Delta/\Delta}$=31.3±12.8% of cells with lagging chromosomes, *n*=265, *P*=0.0049; Spo11-*Arid2*$^{\Delta/\Delta}$= 22.5±2.68% of cells with lagging chromosomes, *n*=115, *P*=0.0054; data were obtained from three different mice per strain) (Fig. 2Ag,h and Fig. 2B). Notably, a number of cells undergoing division II were defective. These cells apparently underwent anaphase but then arrested, resulting in multinucleated cells, and few rounded and elongated spermatids (Fig. 2Ai,l,m). We also performed Hematoxylin and Eosin analysis in 4-month-old Spo11-*Arid2*$^{\Delta/\Delta}$ and littermate control testis. The results showed a similar phenotype to that observed in 2-month-old mice, with abundant lagging chromosomes and cell arrest at meiotic exit (Fig. S5B). The phenotype in testis development we observe agrees with a recent study, in which Arid2 is deleted using Stra8-Cre (Menon et al., 2021).

To further understand why some primary spermatocytes and most secondary spermatocytes in 2-month-old *Arid2*$^{\Delta/\Delta}$ mice show an apparently high rate of abnormal divisions, we analyzed division I and II in spermatocytes in immunostained squashed seminiferous tubules. We used antibodies against tubulin to visualize spindles and DAPI to visualize the chromosomes. SYCP3 and centromeric DAPI signal were used to mark cells at prophase I. Primary (meiotic division I) and secondary (meiosis II) spermatocytes from control males exhibited normally condensed mitotic chromosomes congressing around the spindle equator. Aberrations in chromosome orientation in Ddx4-*Arid2*$^{\Delta/\Delta}$ were evident as different conformations were observed. The chromosome congression failure phenotype was accompanied by gross spindle aberrations, e.g. grossly unequal poles, extremely elongated spindles and three polar spindles (Fig. 2C,D).

SYCP3, SYCP1 and γH2AX immunostaining can be used to precisely identify primary spermatocytes in testis sections. SYCP3 and SYCP1 are part of the synaptonemal complex: a

Development (2022) 149, dev199967. doi:10.1242/dev.199967

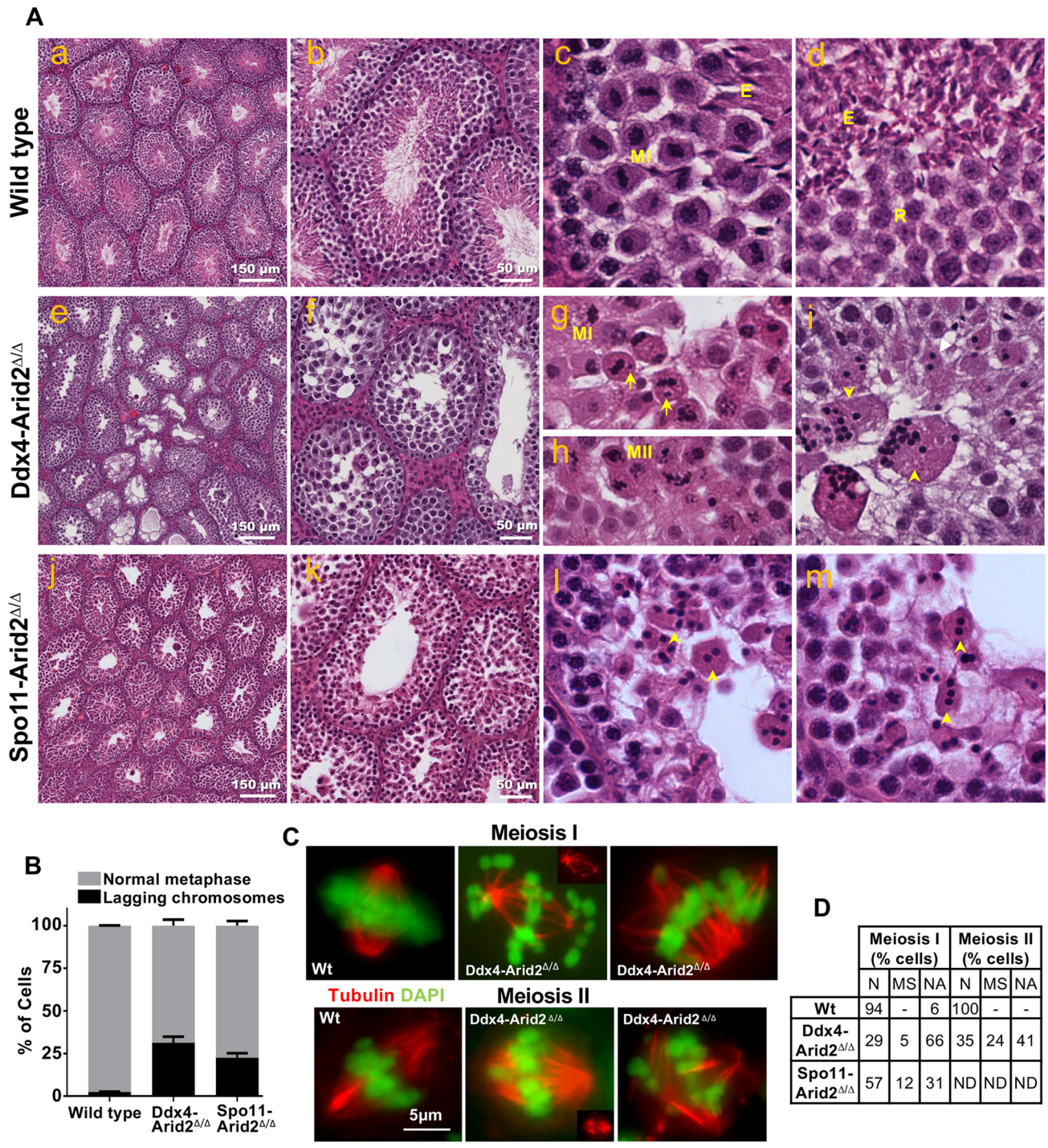

	Meiosis I (% cells)			Meiosis II (% cells)		
	N	MS	NA	N	MS	NA
Wt	94	-	6	100	-	-
Ddx4-Arid2$^{\Delta/\Delta}$	29	5	66	35	24	41
Spo11-Arid2$^{\Delta/\Delta}$	57	12	31	ND	ND	ND

Fig. 2. Gamete developmental impairment in Arid2 knockout mice originates from spindle assembly and microtubule-chromosome attachment defects. (A) Meiosis is arrested at the end of prophase I and II in 2-month-old *Arid2*$^{\Delta/\Delta}$ spermatocytes. Hematoxylin and Eosin staining corresponding to (a-d) wild type; (e-i) Ddx4-*Arid2*$^{\Delta/\Delta}$; and (j-m) Spo11-*Arid2*$^{\Delta/\Delta}$. (g) Cells at metaphase I show lagging chromosomes (some examples are highlighted with arrows). (h) Cells arrested at the second meiotic division showing abnormal chromosome figures. (i) Gigantic polynucleated cells (some examples are indicated with arrowheads) apparently formed after the second meiotic division. MI, metaphase I; MII, metaphase II; E, elongated spermatids; R, rounded spermatids. (B) Quantitation of lagging chromosomes assessed in Hematoxylin and Eosin stained 2-month-old mouse testis sections. Wild type (mean±s.d.) 2.5±0.024% of cells with lagging chromosomes, *n*=122 total cells counted; Ddx4-Arid2$^{\Delta/\Delta}$ 31.3±12.8% of cells with lagging chromosomes, *n*=265 cells, *P*=0.0049, two-tailed unpaired Student's *t*-test; Spo11-Arid2$^{\Delta/\Delta}$ 22.5±2.68% of cells with lagging chromosomes, *n*=115 cells, *P*=0.0054, two-tailed unpaired Student's *t*-test. Data were obtained from three different mice per strain. (C) Representative images of 2-month-old wild-type and Ddx4-*Arid2*$^{\Delta/\Delta}$ squashed seminiferous tubules immunostained using antibodies against tubulin and DAPI. There are multiple spindles and unaligned chromosomes in knockout samples. (D) Quantitation of chromosome conformations in meiosis I and meiosis II cells at metaphase. N, normal metaphase. NA, metaphases showing abnormal metaphase with non-aligned chromosomes (e.g. chromosomes prematurely at the poles). MS, cells with multiple spindles; ND, non-determined. The data were collected from three different mice of each genotype. Wild-type meiosis I (% of cells, *n*=31 total number of cells counted), *n*=94, NA=6; wild-type meiosis II (*n*=30 total cells counted), *n*=100. Ddx4-*Arid2*$^{\Delta/\Delta}$ meiosis I (% of cells, *n*=84 total cells counted), *n*=29, MS=5, NA=66; Ddx4-*Arid2*$^{\Delta/\Delta}$ meiosis II (% of cells, *n*=34 total cells counted), *n*=35, MS=24, NA=41. Spo11-Arid2$^{\Delta/\Delta}$ meiosis I (% of cells, *n*=35 total cells counted), *n*=57, MS=12, NA=31.

Development (2022) 149, dev199967. doi:10.1242/dev.199967

meiosis-specific zipper-like protein complex that connects one pair of sister chromatids to the homologous pair of sister chromatids. Synaptonemal complex formation starts with polymerization of SYCP3 at chromosome cores at the early prophase stage of leptotene. Later, in zygotene, SYCP1 signal appears at sites where the homologous chromosomes begin to zipper together to form the tripartite synaptonemal complex. The synaptonemal complex is fully assembled in pachytene, which is marked by equal length SYCP3 and SYCP1 along the chromosome cores. Upon pachytene exit, SYCP1 disassembles first from the synaptonemal complex as the meiotic cell progresses through diplotene. Finally, only SYCP3 remains at centromeres when the homologs mount the spindle and separate to the opposite poles of the dividing spermatocyte. During these processes, γH2AX marks the entire nuclei in leptotene-zygotene spermatocytes and remains at the sex body in pachytene and diplotene cells. Immunostaining analysis of SYCP1, SYCP3 and γH2AX in testis cuts of 2-month-old *Arid2* knockouts (Ddx4-Cre or Spo11-Cre) revealed no apparent abnormal phenotype when compared with wild type (Fig. 3A).

To determine the precise stages where *Arid2* knockout mice showed abnormal cellular phenotypes, we immunostained paraffin wax-embedded testis sections with cytological markers of primary spermatocytes (SYCP3) and lectin PNA (peanut agglutinin), the latter is an acrosome-specific marker used to characterize spermatids, in combination with DAPI (Fig. 3B) (Yan et al., 2005; Nakata et al., 2015). We observed a significant decrease in S1 spermatids cells in the 2-month-old *Arid2* knockout compared with wild type [wild type=9.9±2.4 number of S1 spermatids per 0.1 mm^2 tubule (mean±s.d.), n=27 tubules, 4793 cells; Ddx4-Cre-Arid2=4.2±1.7 number of S1 spermatids per 0.1 mm^2 tubule, n=33 tubules, 1904 cells, P<0.0001; Spo11-Cre-Arid2=3.6±1.9 number of S1 spermatids per 0.1 mm^2 tubule, n=32 tubules, 1544 cells, P<0.0001, data were obtained from three different 2-month-old mice per strain] (Fig. 3C). Further analysis of spermatid differentiation, from rounded S1 to the most advanced elongated S16, showed that knockout of Arid2 resulted in failure of spermatid differentiation when compared with wild type. We observed typical S1 to S2-S3 in *Arid2*$^{\Delta/\Delta}$ mice but further developmental stages were not recognizable as they were in wild type (Fig. S6). Owing to the arrest of germ cell development at post-meiotic stages, we also observed an increase in primary spermatocytes that accumulate at diplotene stage in *Arid2* knockout compared with wild type (wild-type=3.8±0.65 number of diplotene cells per 0.1 mm^2 tubule, n=17 tubules, 1081 cells; Ddx4-Cre-Arid2=5.9±1.18 number of diplotene cells per 0.1 mm^2 tubule, n=26 tubules, 1733 cells, P<0.0001; Spo11-Cre-Arid2=6.9±1.38 number of diplotene cells per 0.1 mm^2 tubule, n=25 tubules, 1812 cells, P<0.0001) (Fig. 3C).

We then used TUNEL analysis for detection of apoptotic cells to reveal the possible cause of cell loss. In contrast to wild type, in

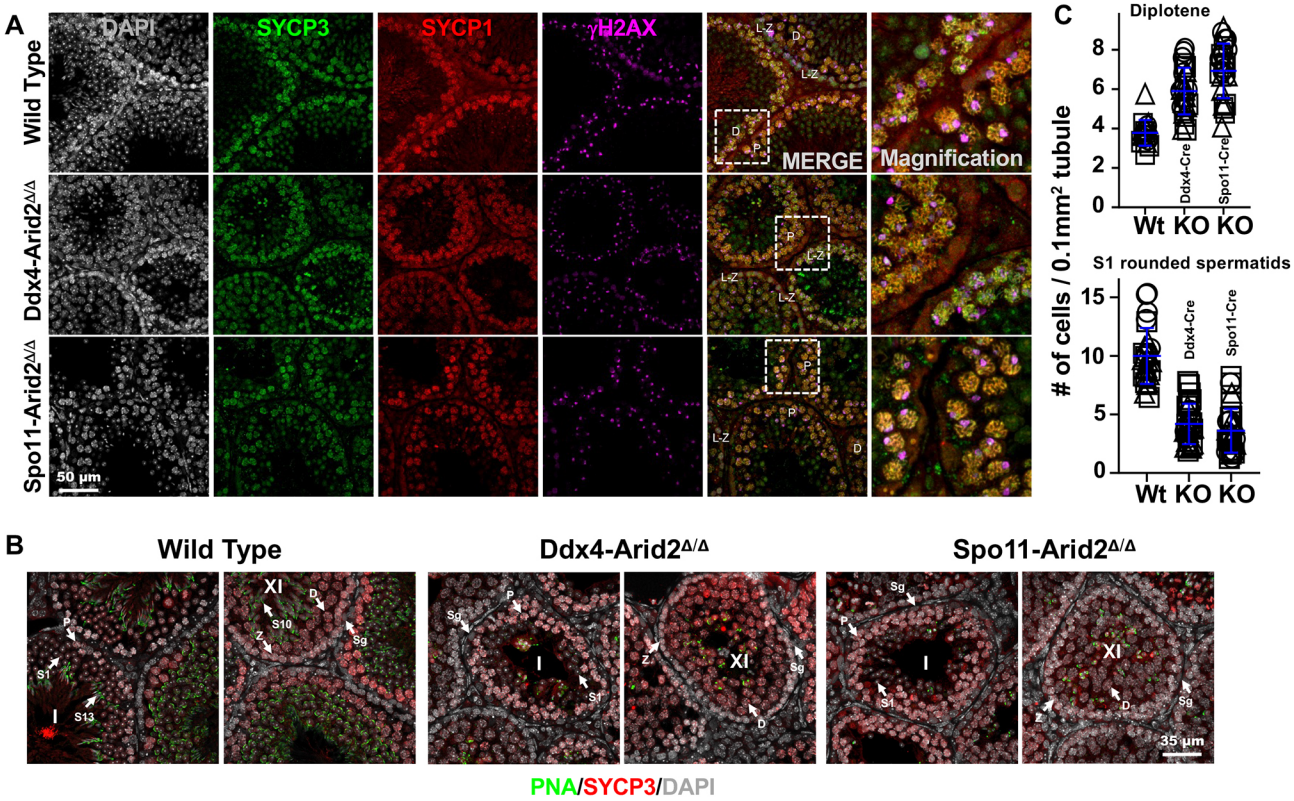

Fig. 3. Characterization of *Arid2* knockout mice gametogenic arrest. (A) Images show SYCP3, SYCP1 and γH2AX immunostaining in paraffin wax-embedded sections of wild-type, Ddx4-*Arid2*$^{\Delta/\Delta}$ and Spo11-*Arid2*$^{\Delta/\Delta}$ mice. L-Z, leptotene-zygotene; D, diplotene; P, pachytene. The images in the far-right panel correspond to the area highlighted by the white square. (B) PNA and SYCP3 immunostaining in wild-type, and Ddx4-Arid2 and Spo11-Arid2 knockout mice. Note the reduction in the number of S1 spermatids and the accumulation of cells at diplotene in tubules type I and XI in *Arid2* knockouts when compared with wild type. S1-S13 indicate different types of spermatids. (C) Quantification of diplotene cells and S1 spermatids (number of cells per 0.1 mm^2 of tubule). Diplotene (mean±s.d.) 3.8±0.65, n=17 tubules, 1081 cells; Ddx4-Cre-Arid2 5.9±1.18, n= 26 tubules, 1733 cells, two-tailed unpaired Student's t-test P<0.0001; Spo11-Cre-Arid2 6.9±1.38, n= 25 tubules, 1812 cells, two-tailed unpaired Student's t-test P<0.0001). S1 rounded spermatids, wild type (mean±s.d.) 9.9±2.4, n=27 tubules, 4793 cells; Ddx4-Cre-Arid2 4.2±1.7, n= 33 tubules, 1904 cells, two-tailed unpaired Student's t-test P<0.0001; Spo11-Cre-Arid2 3.6±1.9, n=32 tubules, 1544 cells, two-tailed unpaired Student's t-test P<0.0001 (data were obtained from three different 2-month-old mice per strain).

Development (2022) 149, dev199967. doi:10.1242/dev.199967

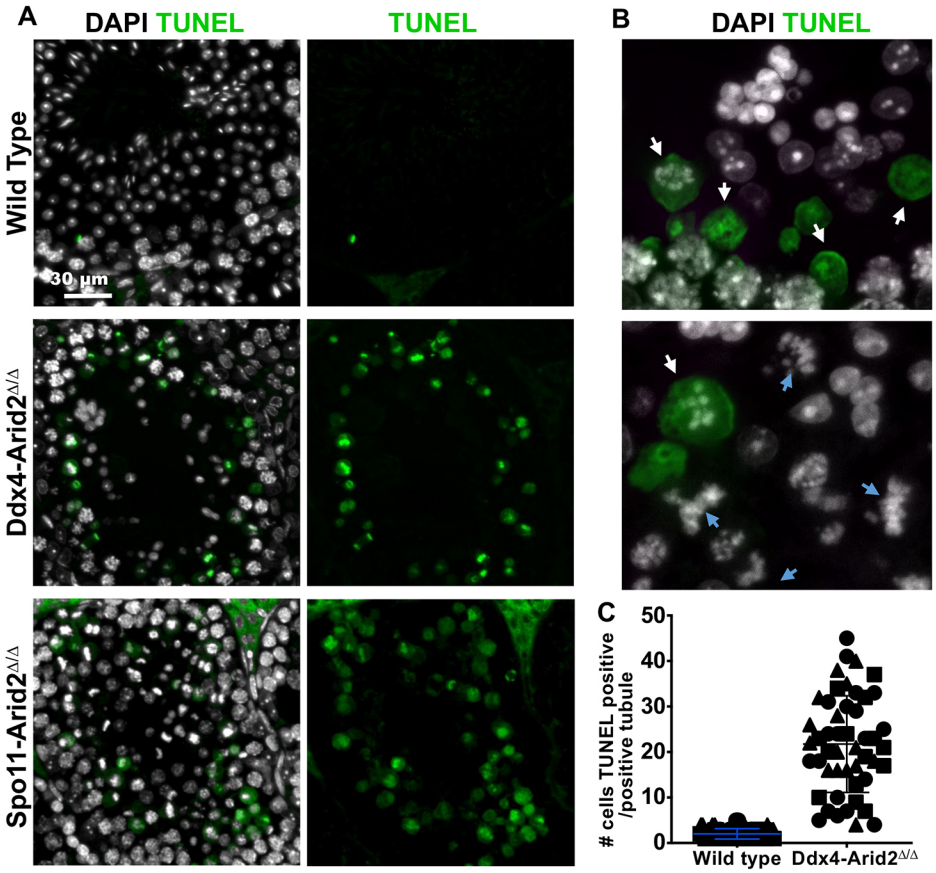

Fig. 4. *Arid2*$^{\Delta/\Delta}$ mice show a higher number of apoptotic cells. (A) Increased number of apoptotic cells positive for TUNEL assay is observed in 2-month-old Ddx4-Arid2 and Spo11-Arid2 knockouts compared with wild type. (B) Higher magnification of apoptotic cells is shown. White arrows indicate examples of TUNEL-positive cells and blue arrows indicates examples of cells at metaphase I with possible lagging chromosomes. (C) Number of apoptotic cells per seminiferous tubule in 2-month-old Ddx4-Arid2 and wild-type mice. Wild-type (2.01±1.15, *n*=95 seminiferous tubules) and *Arid2*$^{\Delta/\Delta}$ (Ddx4-Cre) mice (21.73±10.62, *n*=49; two-tailed unpaired Student's *t*-test $P>0.0001$). Different symbols in the graph correspond to data collected from three mice of each phenotype.

which only occasional apoptotic cells are present, seminiferous tubules of 2-month-old *Arid2*$^{\Delta/\Delta}$ mice showed substantial apoptosis in spermatocytes at metaphase-anaphase (Fig. 4A-C) with some cells surviving and differentiating into rounded and elongated spermatids.

In summary, tissue analysis suggests that spermatogenesis is apparently normal until the end of prophase I, when some spermatocytes show defects in metaphase-anaphase I. The spermatocytes that survive experience severe apoptosis and defects in the second meiotic division.

Arid2 deletion results in overexpression of aurora B kinase centromere protein. Chromosome congression and spindle aberrations, which are characteristic of spermatocytes in Arid2$^{\Delta/\Delta}$ mice, likely originate from a failure of chromosomes to form stable chromosome-spindle attachments. This may be caused by deregulation of structural or regulatory proteins at the centromere and/or kinetochore. To test this, we analyzed the level of expression of known regulators of the spindle-chromosome attachments: aurora B kinase, survivin and PLK1 (polo like kinase I). Aurora B kinase regulates chromosome segregation and cytokinesis, and is a master regulator of bipolar attachment of spindle microtubules to kinetochores (Funabiki, 2019). Evidence from several experimental models suggests that aurora B kinase is physically associated with the inner centromere protein INCENP and with surviving, forming the chromosome passenger domain (Trivedi and Stukenberg, 2020; Saurin, 2018). PLK1 is a key component of eukaryotic cell division, acting dynamically to regulate spindle assembly, microtubule-kinetochore attachment and cytokinesis (Colicino and Hehnly, 2018). PLK1 has also shown to be required for meiotic prophase exit (Jordan et al., 2012).

Western blot analysis of total testis extract from wild type and *Arid2*$^{\Delta/\Delta}$ 2-month-old mice (Ddx4-Cre or Spo11-Cre) revealed a substantial increase in the amount of aurora B kinase protein in *Arid2*$^{\Delta/\Delta}$ mice compared with wild type, but no changes were observed for survivin and PLK1 (Fig. 5A and Fig. S7A,B). We also analyzed expression of aurora B kinase in *Arid2* knockout and wild-type mice by qPCR. Surprisingly, we observed a reduction of aurora B kinase mRNA in the Spo11-*Arid2* knockout compared with wild type (Fig. S7C). Our results indicate that, despite the negative effect of ARID2 depletion on aurora B kinase RNA levels, aurora B kinase protein remains elevated in the *Arid2* mutant. It is possible that this result may be caused by ARID2 modulating at both aurora B kinase transcriptional and protein degradation levels.

Aurora B kinase phosphorylates the Ser 10 residue of histone H3 at G2/MI transition. Changes in aurora B kinase are expected to result in increased phosphorylated H3 at the centromeres in diplotene spermatocytes, where the aurora B kinase activity is first detected. In agreement with results in Fig. 5A, we observed a striking increase in immunofluorescence intensity corresponding to Ser 10 phosphorylated histone H3 in diplotene spermatocytes of Ddx4-*Arid2*$^{\Delta/\Delta}$ compared with wild type (Fig. 5B), which suggest an increased level of aurora B kinase activity.

To test whether localization and protein levels of aurora B kinase were altered in *Arid2*$^{\Delta/\Delta}$ cells, we performed immunolocalization of aurora B kinase in paraffin wax-embedded testis sections (Fig. 5C). There were no changes in aurora B kinase recruitment to centromeres. However, we observed a significant increase in aurora B kinase signal in *Arid2* knockout (Ddx4-*Arid2*$^{\Delta/\Delta}$, 142.5±63.7 aurora B kinase fluorescence intensity, *n*=421 cells obtained from 3 mice, two-tailed Student's *t*-test, $P<0.0001$. Spo11-*Arid2*$^{\Delta/\Delta}$, 126.0±57.9 aurora B

Development (2022) 149, dev199967. doi:10.1242/dev.199967

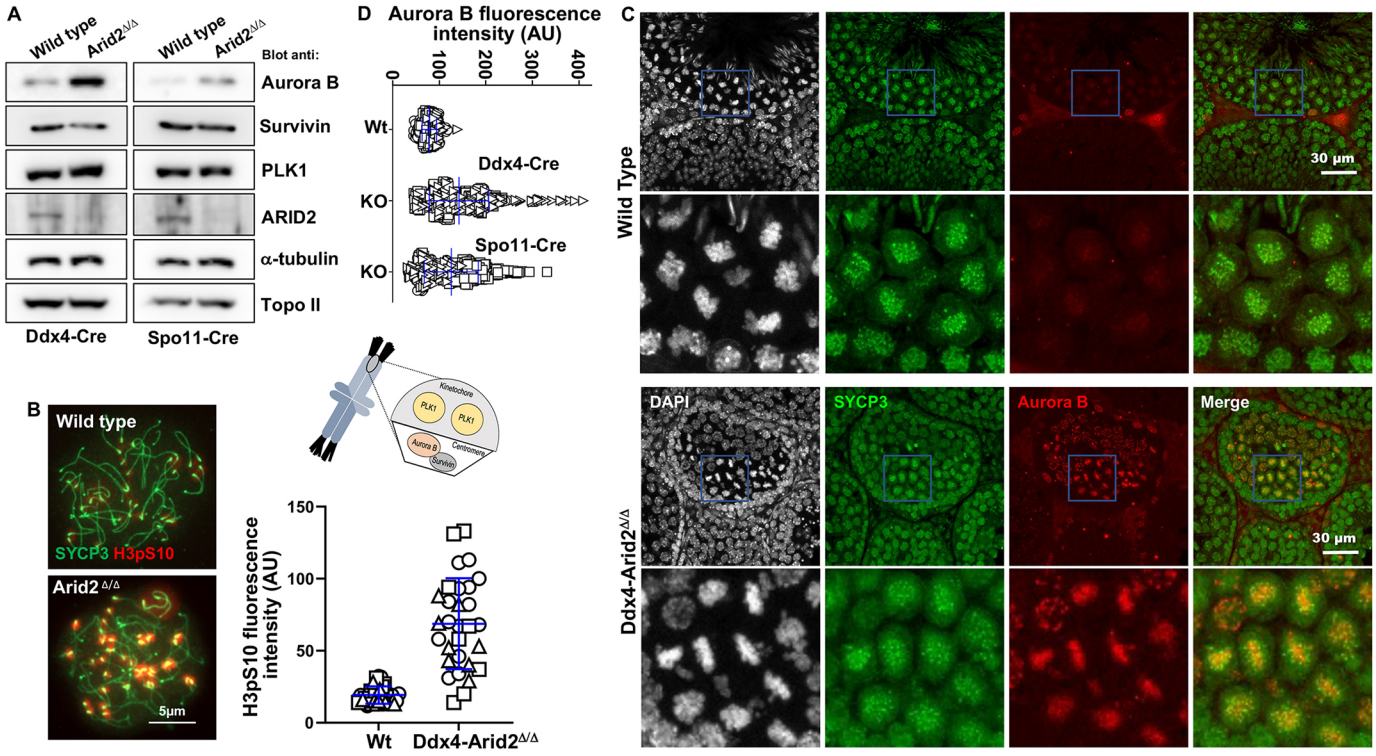

Fig. 5. Defective spindle formation, abnormal chromosome-spindle attachment and increased aurora B kinase at centromeres in *Arid2*$^{\Delta/\Delta}$ testis. (A) Western blots show an increase in aurora B kinase in 2-month-old *Arid2*$^{\Delta/\Delta}$ testis compared with wild type. The diagram shows distribution of PLK1, aurora kinase B and survivin at the centromeric chromosome area. (B) Mouse spermatocyte chromosome spreads from *Arid2*$^{\Delta/\Delta}$ show increased H3pS10 intensity at centromeres in diplotene cells. Antibodies against SYCP3 were used as a marker for the chromosome axis. Quantitation of H3pS10 fluorescent intensity is also shown [wild type (arbitrary units, mean±s.d.) 19.26±6.04, *n*=30 total cell counted, Ddx4-*Arid2*$^{\Delta/\Delta}$ 68.70±31.57, *n*=30 total cell counted; *P*<0.0001, two-tailed unpaired Student's *t*-test (data were obtained from three mice of each phenotype)]. (C) Representative images of paraffin wax-embedded testis sections immunostained for SYCP3 and aurora B kinase in wild-type and Ddx4-Arid2 knockout mice (also see Spo11-Arid2 knockout in Fig. S8A). Cells transitioning metaphase-anaphase I are immunostained for SYCP3. (D) Quantitation corresponding to aurora B kinase immunostaining in metaphase spermatocyte nuclei of wild type, Ddx4-Arid2 and Spo11-Arid2 knockout mice shown in C. Ddx4-*Arid2*$^{\Delta/\Delta}$ (arbitrary units, mean±s.d.) 142.5±63.7, *n*=421 total cells counted obtained from three mice; *P*<0.0001, two tailed two-tailed unpaired Student's *t*-test. Spo11-*Arid2*$^{\Delta/\Delta}$ 126.0±57.9, *n*=493 obtained from three different mice; *P*<0.0001, two-tailed unpaired Student's *t*-test compared with wild-type controls (78.8±15.5 relative fluorescence intensity, *n*=373 cells obtained from three different 2-month-old mice).

kinase fluorescence intensity, *n*=493 obtained from 3 different mice, two tailed Student's *t*-test, *P*<0.0001) compared with wild-type controls (78.8±15.5 aurora B kinase fluorescence intensity, *n*=373 cells obtained from three different 2-month-old mice) (Fig. 5C,D and Fig. S8A). We confirmed these results by analyzing immunolocalization of aurora B kinase in squashed seminiferous tubules. Like wild type, knockout cells exhibiting SYCP3 at centromeres (a marker of cells at metaphase-anaphase I) also were positive for aurora B kinase (Fig. S8Ba,b) or PLK1 (Fig. S8Bd,e). We also observed some cells in Ddx4-*Arid2*$^{\Delta/\Delta}$ spermatocytes with condensed chromosomes, but with no SYCP3, aurora B kinase or PLK1 immunostaining (Fig. S8Bc,f). However, PLK1-negative cells were positive for TUNEL staining (Fig. S8C), indicating that absence of PLK1 (and possibly aurora B kinase) is likely caused by protein degradation in these apoptotic cells. Together our results suggest that the increase in aurora B kinase activity may be the cause of non-functional centromeres and kinetochores, resulting in impaired chromosome-spindle attachments.

Histological evaluation and differences in cellular phenotypes suggest that at least some ARID2 and BRG1 functions may be required at different stages of spermatogenesis

Prompted by the contrasting phenotypic differences we found in *Arid2*$^{\Delta/\Delta}$ mice compared with that previously described for *Brg1*$^{\Delta/\Delta}$ mice (Kim et al., 2012; Wang et al., 2012), we performed a comparative characterization of both phenotypes at both histological and cellular levels. To this end, we first assessed the stage of gametogenesis arrest in Ddx4-Brg1 knockout Hematoxylin and Eosin-stained paraffin wax-embedded sections. In contrast to Spo11/Ddx4-*Arid2*$^{\Delta/\Delta}$ testis, in which cell arrest is first apparent at meiotic exit (Fig. 2A), *Brg1*$^{\Delta/\Delta}$ testes showed cell developmental arrest at the pachytene stage of meiosis I (Fig. 6A).

In agreement with previously published work (Kim et al., 2012), an earlier arrest during prophase of meiosis I in Ddx4-*Brg1*$^{\Delta/\Delta}$ cells resulted in accumulation of γH2AX immunosignal, which indicates a possible defect in the homologous recombination-dependent repair of DSBs (Fig. 6B). Defects in the repair of DSBs usually result in defects in the interaction of homologous chromosomes. Indeed, in Ddx4-*Brg1*$^{\Delta/\Delta}$ cells we observed that homologous chromosome synapsis is deficient (evaluated using SYCP3 immunostaining). In sharp contrast, and similar to wild type, *Arid2*$^{\Delta/\Delta}$ cells at pachytene stage showed normal chromosome synapsis and γH2AX immunosignal located only at the X-Y chromosomes (Fig. 6B,C).

Our results indicate that *Brg1*$^{\Delta/\Delta}$ activates a cell checkpoint leading to spermatocyte arrest at an early pachytene-like stage. In contrast, ARID2 functions at later stages of prophase and/or at the time of formation of the first meiotic spindle. However, in this case a

Development (2022) 149, dev199967. doi:10.1242/dev.199967

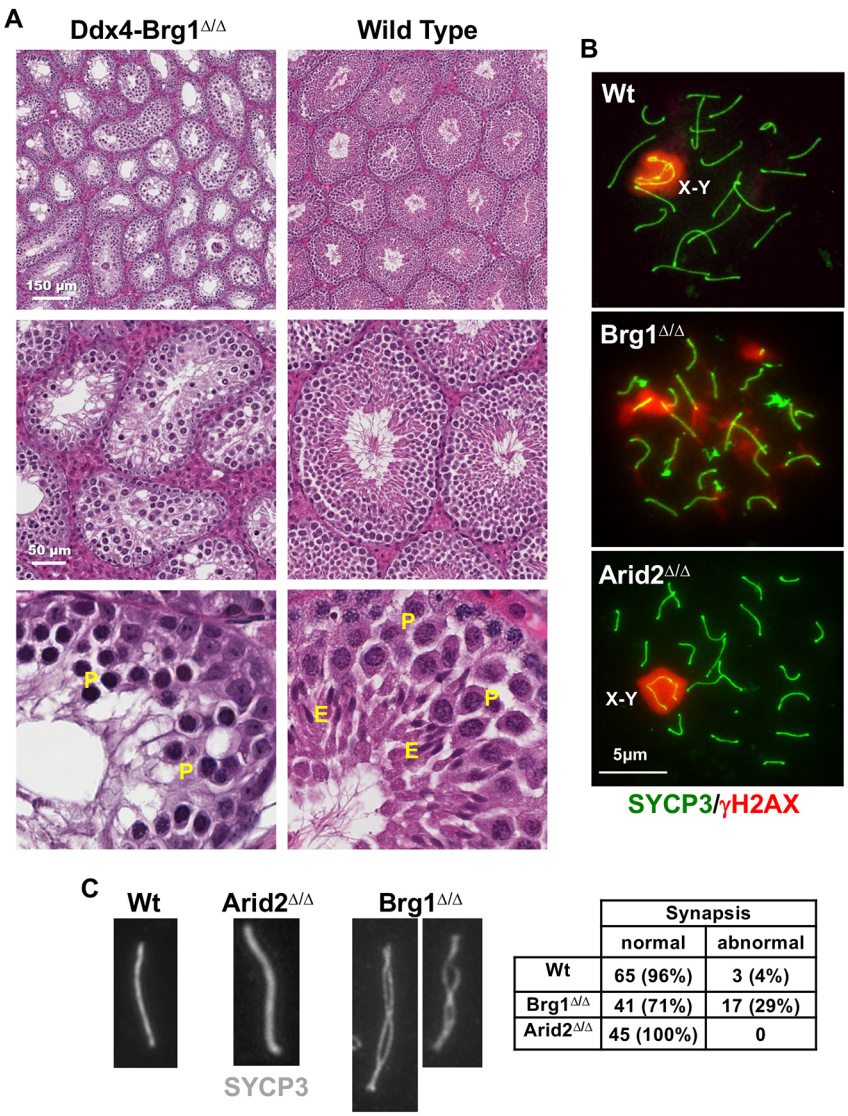

	Synapsis	
	normal	abnormal
Wt	65 (96%)	3 (4%)
Brg1Δ/Δ	41 (71%)	17 (29%)
Arid2Δ/Δ	45 (100%)	0

Fig. 6. Comparative analysis of *Brg1*$^{Δ/Δ}$ and *Arid2*$^{Δ/Δ}$ testes. (A) Hematoxylin and Eosin stained testes sections of wild-type and Ddx4-Brg1 knockout. P, pachytene; E, elongated spermatids. There is arrest at pachynema in Ddx4-*Brg1*$^{Δ/Δ}$. (B) Representative chromosome spreads obtained from 2-month-old wild-type, Ddx4-*Brg1*$^{Δ/Δ}$ and Ddx4-*Arid2*$^{Δ/Δ}$ mice. The extent of γH2AX staining in *Brg1*$^{Δ/Δ}$ is indicative of deficient DSB repair. (C) Representative images of chromosomes and quantitation corresponding to normal and abnormal synapsis in wild-type, Ddx4-*Brg1*$^{Δ/Δ}$ and Ddx4-*Arid2*$^{Δ/Δ}$ mice (number of cells and corresponding percentage are represented in the table). Data were obtained from three mice of each genotype. Wild type, *n*=68 total counted cells; *Brg1*$^{Δ/Δ}$, *n*=58 total counted cells; *Arid2*$^{Δ/Δ}$, *n*=45 total counted cells. Data were obtained from three different 2-month-old mice.

substantial number of cells bypass the cell spindle checkpoint (which leads to spermatocyte arrest at diakinesis) and progress to the second meiotic division.

ARID2 and PBRM1 form a complex that is independent of BRG1 and some ARID2 functions are independent of BRG1

Until recently, PBAF was considered to be a functional entity with a relatively fixed composition of subunits. However, the process of PBAF assembly includes different intermediate complexes (Mashtalir et al., 2018), which may have distinct functions, and we observed that ARID2 participates in biochemically distinct complexes co-existing in somatic cell nuclei (de Castro et al., 2017). To test whether PBAF components exist in distinct complexes in mouse spermatocytes and to determine the subunit composition of such complexes, we used testes lysates obtained from enriched fractions of zygotene and diplotene cells to perform immunodepletion of BRG1 followed by ARID2 immunoprecipitation and analysis by western blot. The results show that BRG1 co-immunoprecipitated with PBAF/BAF core components (i.e. SMARCC2, SMARCC1, SMARCE1 and SMARCB1) and PBAF-specific components (ARID2 and PBRM1), revealing the composition of BRG1-containing canonical PBAF complexes in meiosis (Fig. 7A). ARID2 immunoprecipitated fractions performed on BRG1 immunodepleted samples showed that some PBRM1 and SWI/SNF subunits (SMARCC2, SMARCE1 and SMARCB1) interact with the fraction of ARID2 that is not associated with BRG1. The results indicate that ARID2 and PBRM1 form a complex that is independent of BRG1 (Fig. 7A).

To determine whether the ARID2 function required for chromosome segregation at later stages of meiosis is independent of BRG1, and to test whether BRG1 has an additional function later in meiosis, we generated Spo11-Brg1 knockout mice. In contrast to Ddx4-Brg1, in which Brg1 alleles are deleted in prospermatogonia, it is expected that Spo11-Cre will delete Brg1 in early spermatocytes. This should bypass the requirement for BRG1 in early meiosis but impair a possible later meiotic function. Compared with wild type, Spo11-Brg1 knockout mice show no apparent defect in gamete development and meiosis (Fig. 7B-D and Fig. S9). The results indicate that BRG1 is indispensable only at earlier stages of prophase I and that an ARID2 function at later meiotic stages is independent of BRG1. Taken together, the results support a model in which biochemical and functional distinct PBAF complexes act at different stages of gamete development (Fig. 7E).

Development (2022) 149, dev199967. doi:10.1242/dev.199967

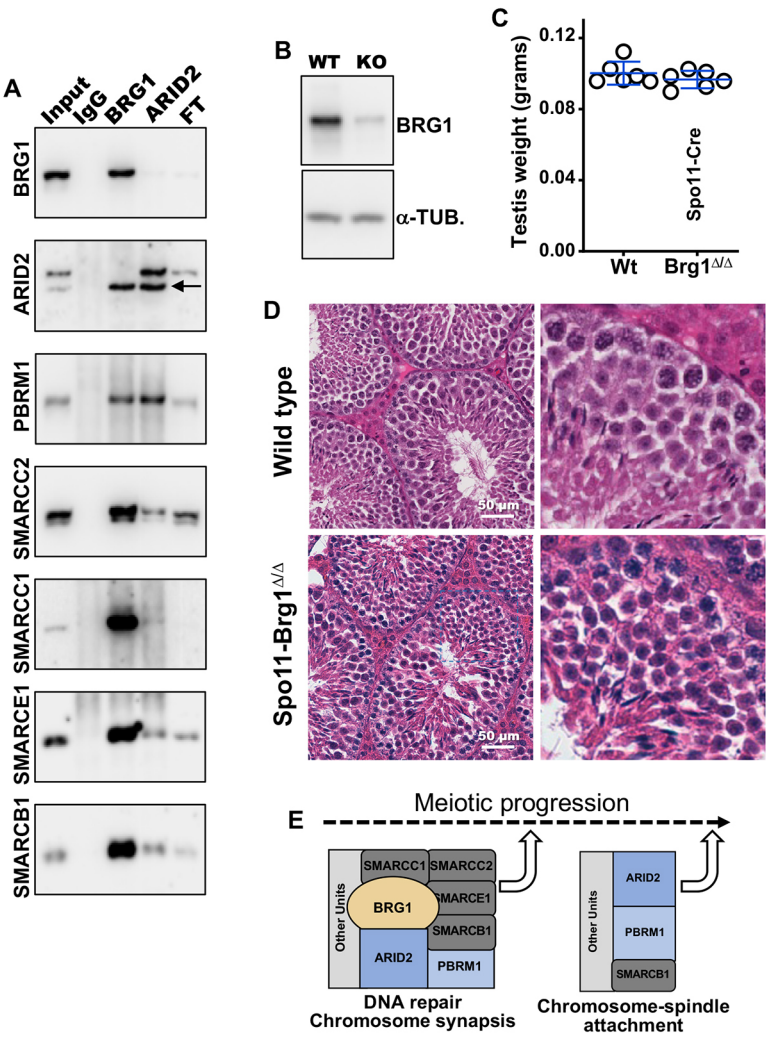

Fig. 7. BRG1-independent PBAF complexes formed by ARID2 and PBRM1. (A) Immunoprecipitation followed by western blotting analysis of synchronized enriched fractions of zygotene spermatocytes. (B) Western blot showing depletion of BRG1 in zygotene- and diplotene-enriched spermatocyte fractions from Spo11-Cre mice. (C) Quantitation of testis weight from 2-month-old mice is also shown. Wild type (mean±s.d.) 0.100±0.0049 g, n=6 testes from 3 mice) and Spo11-Brg1$^{\Delta/\Delta}$ males (0.097±0.0065 g, n=6 testes from 3 mice; P=0.331, two-tailed unpaired Student's t-test). (D) Hematoxylin and Eosin-stained testes sections of Spo11-Cre *Brg1*$^{\Delta/\Delta}$ and wild type. (E) Schematic of the proposed function of BRG1-dependent and -independent PBAF complexes.

DISCUSSION

Increased amounts of aurora B kinase in ARID2 knockout spermatocytes may be the cause of aberrant mitosis, cell arrest and cell apoptosis

Proper distribution of the homologous chromosomes in meiosis I and appropriate distribution of sister chromatids in the second meiotic division require chromosome attachment to the spindle. This is a highly regulated process, as the presence of a single unattached chromosome triggers the spindle-assembly checkpoint, resulting in metaphase arrest (Ballew and Lacefield, 2019; Lane and Kauppi, 2019). Importantly, each kinetochore of each pair of homologs (or sister chromatids in meiosis II) must be connected to opposite spindle poles. Aurora B kinase together with INCENP, survivin and borealin form the chromosomal passenger complex (Trivedi and Stukenberg, 2020), which loads at centromeric regions as early as diplonema with maximum signal at centromeres in metaphase-anaphase. In this context, aurora B kinase plays an essential role in this type of bipolar attachment. In the first meiotic division, the products of recombination hold the homologous chromosome together and in both meiotic divisions, the sister chromatids are bound together by cohesin complexes. Thus, when the homologous chromosomes or sister chromatids are bioriented, the pulling of the microtubules from both spindle poles generates tension. Changes in tension generated by erroneous kinetochore-microtubule attachment are sensed by aurora B kinase, which destabilizes these connections by acting in components from the microtubule-binding site of the kinetochore and activating the spindle attachment checkpoint (Benzi and Piatti, 2020).

We observed that loss of ARID2 resulted in increased amount and activity of aurora B kinase at centromeres, but no effect was observed in other centromere and kinetochore proteins, such as survivin and PLK1. This was accompanied by arrest at metaphase and cell apoptosis. Whereas the absence of aurora B kinase activity leads to chromosome aneuploidy, an excess amount of aurora B kinase causes defective chromosome segregation and threatens cell viability, which have been associated with various types of cancer (Munoz-Barrera and Monje-Casas, 2014). Indeed, elevated activities of aurora B kinase contributes to chromosome number instability in Chinese hamster cells (Ota et al., 2002), and dramatic loss of viability is observed in budding yeast by increasing the expression of aurora B kinase. In yeast, as we observed in mouse meiosis, the increased aurora B kinase seems to promote continuous disruption of chromosome-microtubule attachments and premature collapse of the spindle because of the instability of the spindle midzone (Munoz-Barrera and Monje-Casas, 2014). Our results suggest that ARID2 plays a role in regulating at least one critical activity in chromosome segregation, which explains the phenotype observed at histological and cellular levels. We also noticed that deletion of ARID2 resulted in defects in spindle assembly and chromosome attachment in cells exiting meiosis I and II. Future

Development (2022) 149, dev199967. doi:10.1242/dev.199967

work using specific Cre transgenic mice should address possible differences in the role of ARID2 at meiotic division I and II.

Distinct genetic requirements indicate unique meiotic functions for BRG1 and ARID2

Current models show that SWI/SNF family of chromatin remodelers can be grouped into three subfamilies: BAF, PBAF and ncBAF. These complexes have overlapping subunits, including the ATPase BRG1, but also have unique subunits such as ARID1A/ARID1B (BAF), ARID2/PBRM1/BRD7 (PBAF) and BRD9 (ncBAF). Although SWI/SNF complexes are well known for their role in transcriptional regulation in mitotic dividing cells (Hodges et al., 2016 and references within) less is understood regarding its role in meiotic processes and gametogenesis. Germline-specific ablation of BRG1 or of the PBAF-specific component BRD7 results in gonadal developmental defects (Kim et al., 2012; Wang et al., 2012, 2016). *Brg1* knockout spermatocytes exhibited a prolonged γH2AX immunosignal and an abnormally high level of irregularly distributed RAD51 foci. This is consistent with a role for BRG1 in DNA DSB repair. As expected, this was accompanied by defects in synapsis between homologous chromosome pairs (Kim et al., 2012). Our comparative analysis of *Brg1* and *Arid2* knockout mice phenotypes revealed their individual unique contributions throughout male mouse gametogenesis. Coincidental with previous results, *Brg1* deletion resulted in early meiosis I defects, with associated defects in DNA DSB repair and homologous chromosome associations. In striking contrast, *Arid2* deletion does not affect DNA repair or homologous chromosome associations. Instead, this leads to defects in chromosome spindle association occurring at later stages of meiosis I and meiosis II. In agreement with an exclusive role for BRG1 in early prophase I, and a BRG1-independent role for ARID2 in meiosis, deletion of Brg1 using Spo11-Cre, which bypasses an early meiotic requirement of BRG1, has no effect in gametogenesis. The distinctive effects of Brg1 versus Arid2 deletion we observed strongly indicate separation of function, which we propose may be explained by the formation of distinct functional and perhaps structurally specific PBAF complexes. These complexes may affect chromatin structure at promoter areas and consequently regulate the specific expression of genes. Further experiments to reveal effects on chromatin structure and gene expression in the mutants we generated will be required to clarify these possible mechanisms. Finally, it is possible that the activity of these complexes containing ARID2 but not BRG1 could be independent of chromatin remodeling.

ARID2 and PBRM1 form both a canonical PBAF complex and a BRG1-independent PBAF complex

Our results indicate that ARID2 and PBRM1 form part of a PBAF complex that is also made up of the catalytic component BRG1 and other core components. However, immunodepletion of specific PBAF complex units followed by western blot analysis show that a substantial amount of ARID2 and PBRM1 form part of a complex that is independent of BRG1 (Fig. 7A). It is possible that ARID2/PBRM1 complexes formed in absence of BRG1 could reflect the formation of an earlier intermediate structure in the assembly pathway of a canonical PBAF complex, as was recently suggested by extensive work on somatic cells (Mashtalir et al., 2018). Regardless, it is tempting to speculate that this ARID2/PBRM1 BRG1-independent complex constitutes a novel non-canonical complex that regulates expression of genes important for specific later meiotic transitions essential for normal progression of meiosis and gametogenesis (Fig. 7E).

MATERIALS AND METHODS

Mice and genotyping

Experiments conformed to relevant regulatory standards guidelines and were approved by the Oklahoma Medical Research Foundation-IACUC (Institutional Animal Care and Use Committee). Protocol number 17-25. Unless specified otherwise, mice analyzed were 2 months old.

To generate ARID2-deficient mice we obtained frozen embryos from EUCOMM, parent cell line JM8.N4 (ES Cells) with C57BL/6N as the strain of origin (http://www.informatics.jax.org/allele/MGI:4433303). In this strain, the L1L2_gt2 cassette was inserted between exons 3 and 4. The cassette is composed of a FRT flanked lacZ/neomycin sequence followed by a loxP site. An additional loxP site is inserted downstream of exon 5 at position 96350375. The critical exon 4 is thus flanked by loxP sites. A conditional (floxed) allele can be created by Flp recombinase expression in mice carrying this allele. Further information on targeting strategies used for this and other IKMC alleles can be found at http://www.informatics.jax.org/mgihome/nomen/IKMC_schematics.shtml. Heterozygous founder mice were obtained by resuscitation and implant of embryos at the Texas A&M Institute for Genomic Medicine. Subsequent crosses to eliminate LacZ-Neo and exon 4 were carried out in house. *Brg1*-floxed mice (*Brg1*$^{fl/fl}$) have been described previously (Sumi-Ichinose et al., 1997). Transgenic Cre recombinase mice Ddx4-Cre$^{FVB\text{-}Tg(Ddx4\text{-}cre)1Dcas/J}$ were purchased from The Jackson Laboratory. Spo11-Cre mice were kindly provided by Dr P. Jordan (Johns Hopkins University Bloomberg School of Public Health, Baltimore, MD, USA). Gonad-specific knockouts and wild-type heterozygotes littermates were obtained from crosses between female homozygous flox/flox mice and male heterozygous Cre/+; Wt/flox. The gonad-specific Cre-mediated recombination in germ cells and, thus, Ddx4/Spo11-Cre carriers cannot transmit the floxed allele, i.e. Ddx4-Cre; *Arid2*$^{Wt/fl}$ mice can only transmit the null (Δ) or wild-type Arid2 alleles.

Genomic DNA was collected from tail tips digested at 95°C in buffer A (25 mM NaOH and 0.2 mM EDTA) for 60 min, and the reactions were stopped by adding buffer B (40 mM Tris, pH 5.0). The supernatant was collected for downstream PCR genotyping with EconoTaq PLUS GREEN 2X Master Mix (Biosearch Technologies, 30033-1), according to the manufacturer's instructions. Sequences of primers and size of products are provided in Table S2. All experiments conformed to relevant regulatory standards guidelines and were approved by the Oklahoma Medical Research Foundation-IACUC (Institutional Animal Care and Use Committee).

Histology and immunostaining

Testes were dissected, fixed in 10% neutral-buffered formalin (Azer Scientific, B-PFNBF-20) and processed for paraffin wax embedding. After sectioning (5-15-µm), tissues were positioned on microscope slides and analyzed using Hematoxylin and Eosin using standard protocols. For immunostaining analysis, tissue sections were deparaffinized, rehydrated and antigen was recovered in sodium citrate buffer (10 mM sodium citrate, 0.05% Tween 20, pH 6.0) by heat/pressure-induced epitope retrieval. Incubations with primary antibodies were carried out for 12 h at 4°C in 3% PBS/BSA. Primary antibodies used in this study are detailed in Table S3. After five washes in 1× PBS, slides were incubated for 1 h at room temperature with secondary antibodies. A combination of anti-IgG-conjugates were diluted 1:450. Slides were subsequently counterstained for 3 min with 2 µg/ml DAPI containing Vectashield mounting solution (Vector Laboratories) and sealed with nail varnish. We used and Axiovision SE 64, Zeiss LSM-710 confocal or Nikon C2 confocal for imaging acquisition and processing.

For Hematoxylin and Eosin-stained samples, testes were removed and fixed overnight in 10% neutral-buffered formalin. Serial sections from paraffin wax-embedded testes or ovaries were positioned on microscope slides and analyzed using either Hematoxylin and Eosin staining or a TUNEL assay (Roche).

Chromosome spreads

We used established experimental approaches to visualize chromosomes in chromosome surface spreads (Peters et al., 1997). Incubation with primary antibodies occurred for 12 h at 4°C in 1× PBS plus 2% BSA. Slides were incubated with primary antibodies followed by three washes in 1× PBS and

Development (2022) 149, dev199967. doi:10.1242/dev.199967

then incubated for 1 h at room temperature with secondary antibodies. A combination of fluorescein isothiocyanate (FITC)-conjugated goat anti-rabbit IgG (Jackson laboratories) with rhodamine-conjugated goat anti-mouse IgG each diluted 1:250 were used for simultaneous double immunolabeling. Slides were subsequently counterstained for 3 min with 2 µg/ml DAPI containing Vectashield mounting solution (Vector Laboratories) and sealed with nail varnish. We used an Axiovision SE 64 (Carl Zeiss) for imaging acquisition, visualization for immunosignal counting and processing.

Preparation and analysis of squashed seminiferous tubules

Seminiferous tubules were loosened using forceps, washed twice in PBS and placed in PFB (permeabilization/fixative buffer: 2% paraformaldehyde, 0.1% Triton X-100 in PBS) for 5 min. Small pieces of seminiferous tubules (15-20 mm) were positioned on poly-lysine slides coated in 100 µL of PFB. Coverslips (22×22 - 1.5 mm) were placed and enough force was applied to disperse spermatocytes from the seminiferous tubules. Immediately afterwards, the slide was submerged in liquid N_2 for 1 min, the coverslip was removed and the slides containing the seminiferous tubules were placed in PBS until use. Immunolabeling is described above.

Western blot

After testis detunication, seminiferous tubules were washed in ice-cold 1× PBS and lysed in protein extraction buffer containing 0.1% Nonidet P-40, 50 mM Tris-HCl (pH 7.9), 150 mM NaCl, 3 mM $MgCl_2$, 3 mM EDTA, 10% glycerol, 1 mM DTT, 1 mM PMSF and protease inhibitors (ThermoFisher Scientific, A32965). For total lysates, the samples were sonicated (three pulses of 10 s) using micro ultrasonic cell disrupter (Kontes). The relative amount of protein was determined measuring absorbance at 260 nm using NanoDrop 2000c spectrophotometer (ThermoFisher Scientific). Proteins were solubilized with 2× sample buffer [4% SDS, 160 mM Tris-HCl (pH 6.8), 20% glycerol, 4% mM β-mercaptoethanol and 0.005% bromphenol blue] and 30-50 µg/lane of sample were separated by 4-15% gradient Tris-acetate SDS-PAGE and electro-transferred to PVDF membrane (Sigma Aldrich, 3010040001). To obtain a fraction enriched in chromatin-bound proteins, after lysis in protein extraction buffer, samples were centrifuged, pellets containing chromatin-bound proteins were washed twice in the same buffer and proteins were solubilized with sample buffer. The blots were probed with individual primary antibodies and then incubated with HRP-conjugated goat anti-mouse or -rabbit antibody as required. In all blots, proteins were visualized by enhanced chemiluninescence and images acquired using Western Blot Imaging System c600 (Azure Biosystems). ImageJ software was used for quantification of non-saturated bands and α-tubulin was used for normalization. Antibodies used are detailed in Table S3.

q-PCR

Total RNA was isolated from adult testis (2 months old) with the Direct-zol RNA MiniPrep Plus kit (Zymo Research). RNA (2.0 µg) was oligo-dT primed and reverse transcribed with the high-capacity RNA-to-cDNA kit (Applied Biosystems). Exon boundaries of *Aurkb* were amplified using TaqMan Assays (Applied Biosystems) as directed by the manufacturer using β-2 macroglobulin as standard. TaqMan Mm01718146_g1 (Aurkb, exon boundary 7-8), Mm01718140_m1 (Aurkb, exon boundary 1-2), and Mm00437762_m1 (β2 microglobulin). Gene expression was normalized with respect to wild type, with wild-type expression levels considered to be 1.

Immunoprecipitation

Co-immunoprecipitation of SWI/SNF complexes were performed using synchronized meiocytes at zygotene or diplotene with few changes (Romer et al., 2018). Seminiferous tubules were loosened using forceps, washed twice with ice-cold PBS, and lysed using ice-cold IP buffer [50 mM Tris-HCl (pH 7.4), 0.1% Nonidet P-40, 150 mM NaCl, 3 mM MgCl2, 3 mM EDTA, 10% glycerol, 1 mM DTT, 1 mM PMSF and protease inhibitors], sheared using a 2 3G needle, incubated on ice for 15 min and centrifugated at 1000 ***g*** for 10 min at 4°C. Supernatant was collected in a separate tube, the pellet was resuspended in IP buffer, disrupted by sonication (three pulses of 10 s) and centrifuged 12,000 ***g***. This second supernatant was combined with the previous one and protein concentration was determined. We used 750 µg of protein (3 µg/µl) for each immunoprecipitation. Lysates were pre-cleared with protein G magnetic beads (BioRad, 161-4023) for 1 h and incubated with 6 µg of antibodies pre-bound to protein G magnetic beads in the following series: rabbit IgG (Jackson ImmunoResearch, 011-000-003), anti-BRG1 and anti-ARID2. Beads were washed four times with IP buffer and twice with ice-cold 1× PBS. Proteins were eluted by boiling the beads with 2× sample buffer and analyzed by SDS-PAGE as described above.

Statistical analyses

Data are presented as mean±s.d. Statistical analysis was performed using Prism Graph statistical software. A two-tailed unpaired Student's *t*-test was used for comparisons between two groups. $P<0.05$ was considered statistically significant.

Acknowledgements

We thank OMRF Bioterium and Imaging facilities for their support.

Competing interests

The authors declare no competing or financial interests.

Author contributions

Conceptualization: R.O.d.C., R.J.P.; Methodology: R.O.d.C.; Validation: R.O.d.D., L.P.d.A., A.C., I.G., R.J.P.; Formal analysis: R.O.d.C., L.P.d.A., I.G., R.J.P.; Resources: R.O.d.C., A.C.; Data curation: I.G.; Writing - review & editing: R.O.d.C., A.C., R.J.P.; Visualization: R.O.d.C., R.J.P.; Supervision: R.J.P.; Project administration: R.J.P.; Funding acquisition: R.J.P.

Funding

This work was supported by the National Institute of General Medicine-National Institutes of Health (R01 GM125803 to R.J.P.) and the Oklahoma Center for the Advancement of Science and Technology (HR20-028 to R.J.P.). Deposited in PMC for release after 12 months.

Peer review history

The peer review history is available online at https://journals.biologists.com/dev/lookup/doi/10.1242/dev.199967.reviewer-comments.pdf.

References

Ballew, O. and Lacefield, S. (2019). The DNA damage checkpoint and the spindle position checkpoint: guardians of meiotic commitment. *Curr. Genet.* **65**, 1135-1140. doi:10.1007/s00294-019-00981-z

Benzi, G. and Piatti, S. (2020). Killing two birds with one stone: how budding yeast Mps1 controls chromosome segregation and spindle assembly checkpoint through phosphorylation of a single kinetochore protein. *Curr. Genet.* **66**, 1037-1044. doi:10.1007/s00294-020-01091-x

Centore, R. C., Sandoval, G. J., Soares, L. M. M., Kadoch, C. and Chan, H. M. (2020). Mammalian SWI/SNF chromatin remodeling complexes: emerging mechanisms and therapeutic strategies. *Trends Genet.* **36**, 936-950. doi:10.1016/j.tig.2020.07.011

Cheng, C. Y. and Mruk, D. D. (2010). The biology of spermatogenesis: the past, present and future. *Philos. Trans. R. Soc. Lond. B Biol. Sci.* **365**, 1459-1463. doi:10.1098/rstb.2010.0024

Colicino, E. G. and Hehnly, H. (2018). Regulating a key mitotic regulator, polo-like kinase 1 (PLK1). *Cytoskeleton (Hoboken)* **75**, 481-494. doi:10.1002/cm.21504

de Castro, R. O., Previato, L., Goitea, V., Felberg, A., Guiraldelli, M. F., Filiberti, A. and Pezza, R. J. (2017). The chromatin-remodeling subunit Baf200 promotes homology-directed DNA repair and regulates distinct chromatin-remodeling complexes. *J. Biol. Chem.* **292**, 8459-8471. doi:10.1074/jbc.M117.778183

Emery, P., Durand, B., Mach, B. and Reith, W. (1996). RFX proteins, a novel family of DNA binding proteins conserved in the eukaryotic kingdom. *Nucleic Acids Res.* **24**, 803-807. doi:10.1093/nar/24.5.803

Funabiki, H. (2019). Correcting aberrant kinetochore microtubule attachments: a hidden regulation of Aurora B on microtubules. *Curr. Opin. Cell Biol.* **58**, 34-41. doi:10.1016/j.ceb.2018.12.007

Hargreaves, D. C. and Crabtree, G. R. (2011). ATP-dependent chromatin remodeling: genetics, genomics and mechanisms. *Cell Res.* **21**, 396-420. doi:10.1038/cr.2011.32

He, L., Tian, X., Zhang, H., Hu, T., Huang, X., Zhang, L., Wang, Z. and Zhou, B. (2014). BAF200 is required for heart morphogenesis and coronary artery development. *PLoS One* **9**, e109493. doi:10.1371/journal.pone.0109493

Helming, K. C., Wang, X. and Roberts, C. W. (2014). Vulnerabilities of mutant SWI/SNF complexes in cancer. *Cancer Cell* **26**, 309-317. doi:10.1016/j.ccr.2014.07.018

Hodges, C., Kirkland, J. G. and Crabtree, G. R. (2016). The many roles of BAF (mSWI/SNF) and PBAF complexes in cancer. *Cold Spring Harb Perspect Med* **6**, a026930. doi:10.1101/cshperspect.a026930

Jordan, P. W., Karppinen, J. and Handel, M. A. (2012). Polo-like kinase is required for synaptonemal complex disassembly and phosphorylation in mouse spermatocytes. *J. Cell Sci.* **125**, 5061-5072. doi:10.1242/jcs.105015

Kakarougkas, A., Ismail, A., Chambers, A. L., Riballo, E., Herbert, A. D., Kunzel, J., Löbrich, M., Jeggo, P. A. and Downs, J. A. (2014). Requirement for PBAF in transcriptional repression and repair at DNA breaks in actively transcribed regions of chromatin. *Mol. Cell* **55**, 723-732. doi:10.1016/j.molcel.2014.06.028

Kim, Y., Fedoriw, A. M. and Magnuson, T. (2012). An essential role for a mammalian SWI/SNF chromatin-remodeling complex during male meiosis. *Development* **139**, 1133-1140. doi:10.1242/dev.073478

Lane, S. and Kauppi, L. (2019). Meiotic spindle assembly checkpoint and aneuploidy in males versus females. *Cell. Mol. Life Sci.* **76**, 1135-1150. doi:10.1007/s00018-018-2986-6

Liu, L., Wan, X., Zhou, P., Zhou, X., Zhang, W., Hui, X., Yuan, X., Ding, X., Zhu, R., Meng, G. et al. (2018). The chromatin remodeling subunit Baf200 promotes normal hematopoiesis and inhibits leukemogenesis. *J Hematol Oncol* **11**, 27. doi:10.1186/s13045-018-0567-7

Manceau, G., Letouze, E., Guichard, C., Didelot, A., Cazes, A., Corté, H., Fabre, E., Pallier, K., Imbeaud, S., Le Pimpec-Barthes, F. et al. (2013). Recurrent inactivating mutations of ARID2 in non-small cell lung carcinoma. *Int. J. Cancer* **132**, 2217-2221. doi:10.1002/ijc.27900

Mashtalir, N., D'Avino, A. R., Michel, B. C., Luo, J., Pan, J., Otto, J. E., Zullow, H. J., McKenzie, Z. M., Kubiak, R. L., St Pierre, R. et al. (2018). Modular organization and assembly of SWI/SNF family chromatin remodeling complexes. *Cell* **175**, 1272-1288. doi:10.1016/j.cell.2018.09.032

Menon, D. U., Shibata, Y., Mu, W. and Magnuson, T. (2019). Mammalian SWI/SNF collaborates with a polycomb-associated protein to regulate male germline transcription in the mouse. *Development* **146**, dev174094. doi:10.1242/dev.174094

Menon, D. U., Kirsanov, O., Geyer, C. B. and Magnuson, T. (2021). Mammalian SWI/SNF chromatin remodeler is essential for reductional meiosis in males. *Nat. Commun.* **12**, 6581. doi:10.1038/s41467-021-26828-1

Mittal, P. and Roberts, C. W. M. (2020). The SWI/SNF complex in cancer - biology, biomarkers and therapy. *Nat Rev Clin Oncol* **17**, 435-448. doi:10.1038/s41571-020-0357-3

Munoz-Barrera, M. and Monje-Casas, F. (2014). Increased Aurora B activity causes continuous disruption of kinetochore-microtubule attachments and spindle instability. *Proc. Natl. Acad. Sci. USA* **111**, E3996-E4005. doi:10.1073/pnas.1408017111

Nakata, H., Wakayama, T., Takai, Y. and Iseki, S. (2015). Quantitative analysis of the cellular composition in seminiferous tubules in normal and genetically modified infertile mice. *J. Histochem. Cytochem.* **63**, 99-113. doi:10.1369/0022155414562045

Ota, T., Suto, S., Katayama, H., Han, Z. B., Suzuki, F., Maeda, M., Tanino, M., Terada, Y. and Tatsuka, M. (2002). Increased mitotic phosphorylation of histone H3 attributable to AIM-1/Aurora-B overexpression contributes to chromosome number instability. *Cancer Res.* **62**, 5168-5177.

Peters, A. H., Plug, A. W., van Vugt, M. J. and de Boer, P. (1997). A drying-down technique for the spreading of mammalian meiocytes from the male and female germline. *Chromosome Res.* **5**, 66-68. doi:10.1023/A:1018445520117

Pulice, J. L. and Kadoch, C. (2016). Composition and function of mammalian SWI/SNF chromatin remodeling complexes in human disease. *Cold Spring Harb. Symp. Quant. Biol.* **81**, 53-60. doi:10.1101/sqb.2016.81.031021

Romer, K. A., de Rooij, D. G., Kojima, M. L. and Page, D. C. (2018). Isolating mitotic and meiotic germ cells from male mice by developmental synchronization, staging, and sorting. *Dev. Biol.* **443**, 19-34. doi:10.1016/j.ydbio.2018.08.009

Ryme, J., Asp, P., Bohm, S., Cavellan, E. and Farrants, A. K. (2009). Variations in the composition of mammalian SWI/SNF chromatin remodelling complexes. *J. Cell. Biochem.* **108**, 565-576. doi:10.1002/jcb.22288

Saurin, A. T. (2018). Kinase and phosphatase cross-talk at the kinetochore. *Front. Cell Dev. Biol.* **6**, 62. doi:10.3389/fcell.2018.00062

Shang, L., Cho, M. T., Retterer, K., Folk, L., Humberson, J., Rohena, L., Sidhu, A., Saliganan, S., Iglesias, A., Vitazka, P. et al. (2015). Mutations in ARID2 are associated with intellectual disabilities. *Neurogenetics* **16**, 307-314. doi:10.1007/s10048-015-0454-0

Sumi-Ichinose, C., Ichinose, H., Metzger, D. and Chambon, P. (1997). SNF2beta-BRG1 is essential for the viability of F9 murine embryonal carcinoma cells. *Mol. Cell. Biol.* **17**, 5976-5986. doi:10.1128/MCB.17.10.5976

Trivedi, P. and Stukenberg, P. T. (2020). A condensed view of the chromosome passenger complex. *Trends Cell Biol.* **30**, 676-687. doi:10.1016/j.tcb.2020.06.005

Wang, W., Xue, Y., Zhou, S., Kuo, A., Cairns, B. R. and Crabtree, G. R. (1996). Diversity and specialization of mammalian SWI/SNF complexes. *Genes Dev.* **10**, 2117-2130. doi:10.1101/gad.10.17.2117

Wang, J., Gu, H., Lin, H. and Chi, T. (2012). Essential roles of the chromatin remodeling factor BRG1 in spermatogenesis in mice. *Biol. Reprod.* **86**, 186. doi:10.1095/biolreprod.111.097097

Wang, H., Zhao, R., Guo, C., Jiang, S., Yang, J., Xu, Y., Liu, Y., Fan, L., Xiong, W., Ma, J. et al. (2016). Knockout of BRD7 results in impaired spermatogenesis and male infertility. *Sci. Rep.* **6**, 21776. doi:10.1038/srep21776

Wilsker, D., Probst, L., Wain, H. M., Maltais, L., Tucker, P. W. and Moran, E. (2005). Nomenclature of the ARID family of DNA-binding proteins. *Genomics* **86**, 242-251. doi:10.1016/j.ygeno.2005.03.013

Xu, F., Flowers, S. and Moran, E. (2012). Essential role of ARID2 protein-containing SWI/SNF complex in tissue-specific gene expression. *J. Biol. Chem.* **287**, 5033-5041. doi:10.1074/jbc.M111.279968

Yan, Z., Cui, K., Murray, D. M., Ling, C., Xue, Y., Gerstein, A., Parsons, R., Zhao, K. and Wang, W. (2005). PBAF chromatin-remodeling complex requires a novel specificity subunit, BAF200, to regulate expression of selective interferon-responsive genes. *Genes Dev.* **19**, 1662-1667. doi:10.1101/gad.1323805

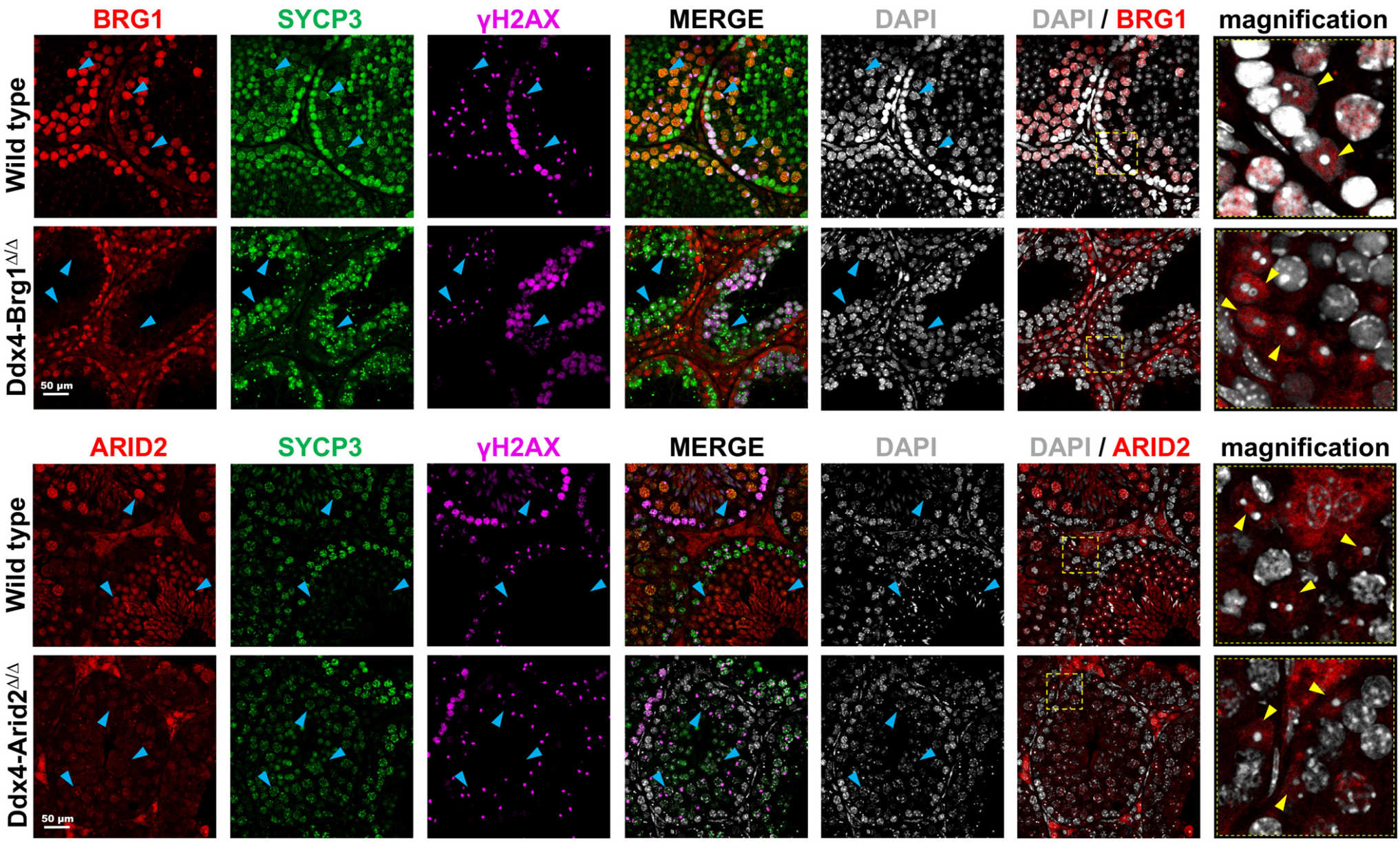

Fig. S1. Immunolocalization of BRG1 and ARID2 in paraffin embedded mouse testis sections. SYCP3 and γH2AX immunostaining serve to classify primary spermatocytes at different stages of prophase I in 2-month-old testis. Blue arrowheads mark examples of positive primary spermatocytes in wild type and examples of primary spermatocytes with negative immunostaining for BRG1 and ARID2 in knockout testis. Magnifications in the far-right panels correspond to the yellow square inserts. Yellow arrowheads show examples of Sertoli cells still expressing BRG1 or ARID2 proteins in both wild type and knockout mice.

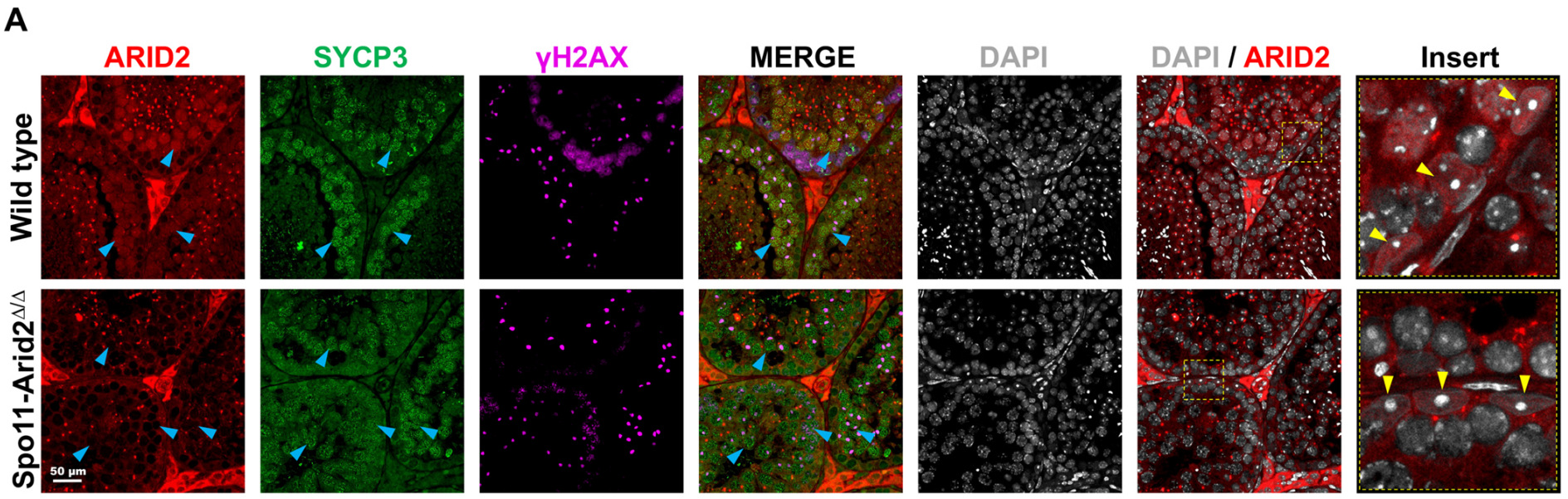

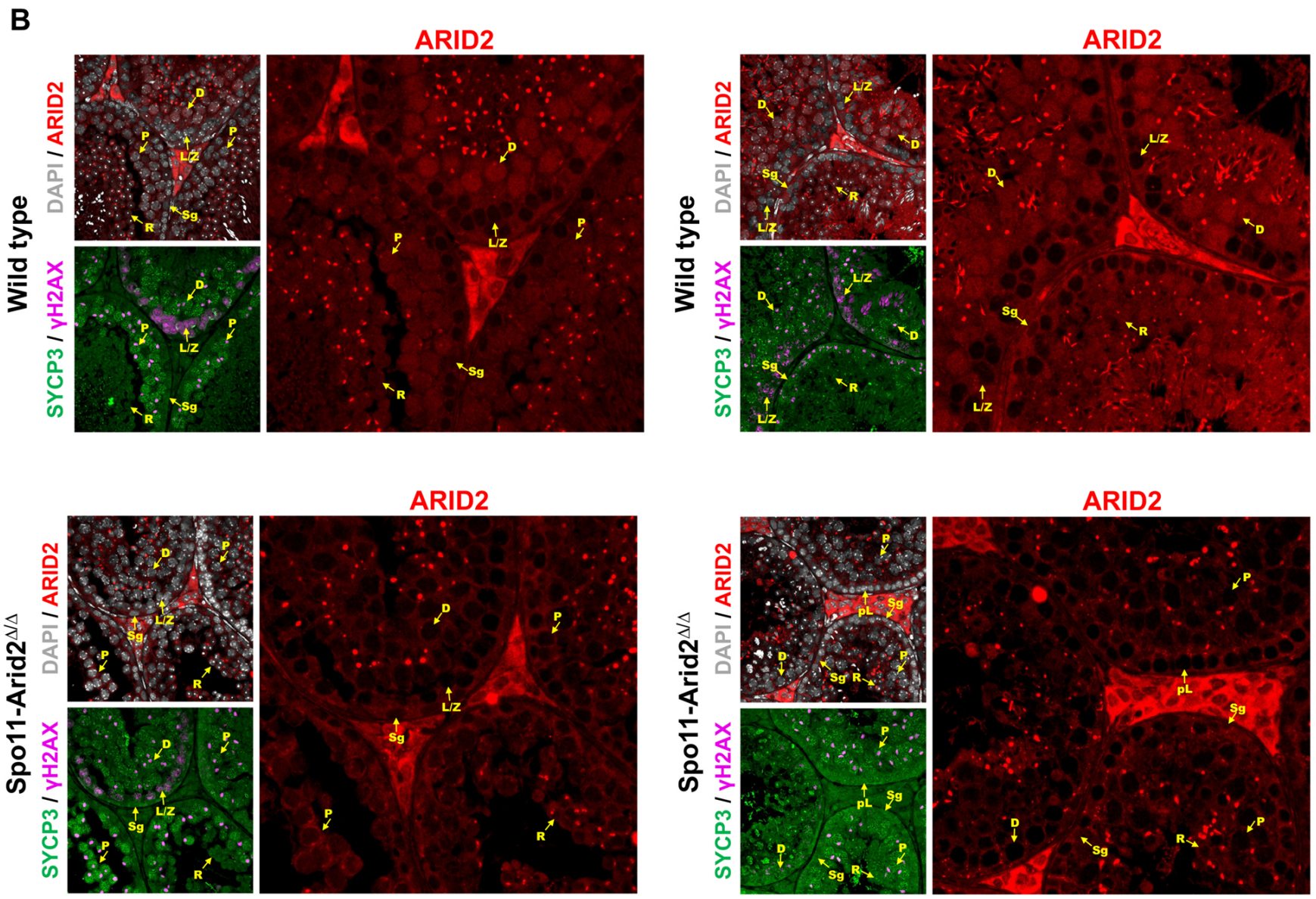

Fig. S2. Analysis of ARID2 immunosignal in testis cuts of wild type and Spo11-Arid2 knockout. A. Paraffin embedded cuts from Spo11-Arid2 knockout and wild type control stained with SYCP3, ARID2, and γH2AX. Blue arrowheads mark examples of primary spermatocytes immunostained with ARID2 in wild type and Arid2 knockout testis. Magnifications in the far-right panels correspond to the yellow square inserts. Yellow arrowheads show examples of Sertoli cells still expressing ARID2 protein in both wild type and knockout mice. **B.** High magnification images showing cells at different stages of spermatogenesis immunostained with the indicated markers. Sg: spermatogonia, pL: pre-leptotene, L/Z: leptotene/zygotene, P: pachytene, D: diplotene, and R: rounded. In these images we observed red foci in both wild type and knockout seminiferous tubules, possibly caused by a different antibody lot used in these experiments.

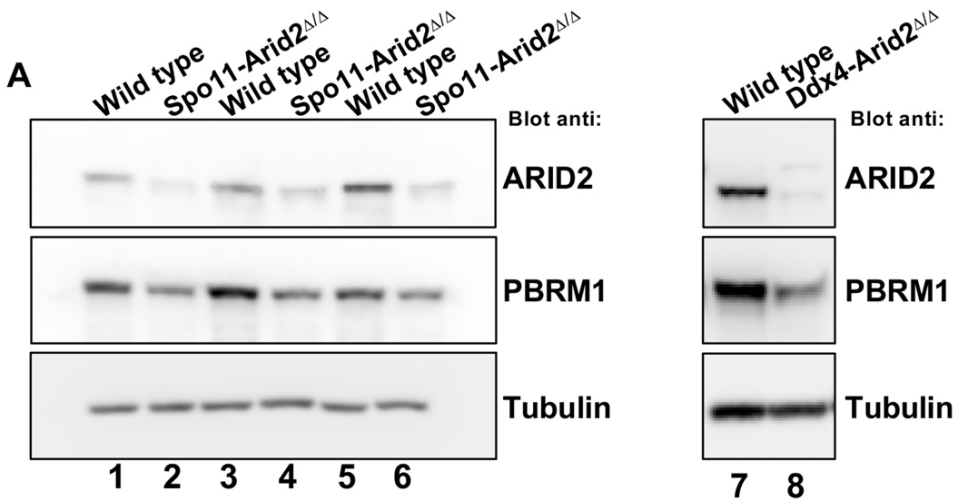

B

Strain	PBRM1	α-Tubulin	KO:WT ratio
Wt (1)	11552	11083	-
Spo11-Arid2$^{\Delta/\Delta}$ (2)	7048	13444	0.74
Wt (3)	16598	12510	-
Spo11-Arid2$^{\Delta/\Delta}$ (4)	8239	13595	0.54
Wt (5)	10284	12063	-
Spo11-Arid2$^{\Delta/\Delta}$ (6)	6191	11633	0.58
Wt (7)	28543	21878	-
Ddx4-Arid2$^{\Delta/\Delta}$ (8)	11724	17572	0.33

C

Strain	PBRM1	α-Tubulin	KO:WT ratio
Wt	5481	16227	-
Ddx4-Arid2$^{\Delta/\Delta}$	3120	14614	0.51
Wt	8435	9127	-
Spo11-Arid2$^{\Delta/\Delta}$	4306	10832	0.61

Fig. S3. Reduction of PBRM1 protein levels in Arid2 knockout mice. A. Western blots showing results for three 2-month-old independent mouse of each wild type and Spo11-Arid2 knockout genotype (lines 1-6). The right panel contain western blot corresponding to an additional example of wild type and Ddx4-Arid2 knockout (lines 7, 8). **B.** Quantitation corresponding to PBRM1 and tubulin band density in western blots shown in A. To determine PBRM1 expression changes, PBRM1 immunosignal intensity was normalized to the corresponding tubulin values, followed by KO/Wt ratio calculati on. **C.** Quantitation corresponding to band density in western blots shown Figure 1A. PBRM1 expression changes were calculated as describe in B.

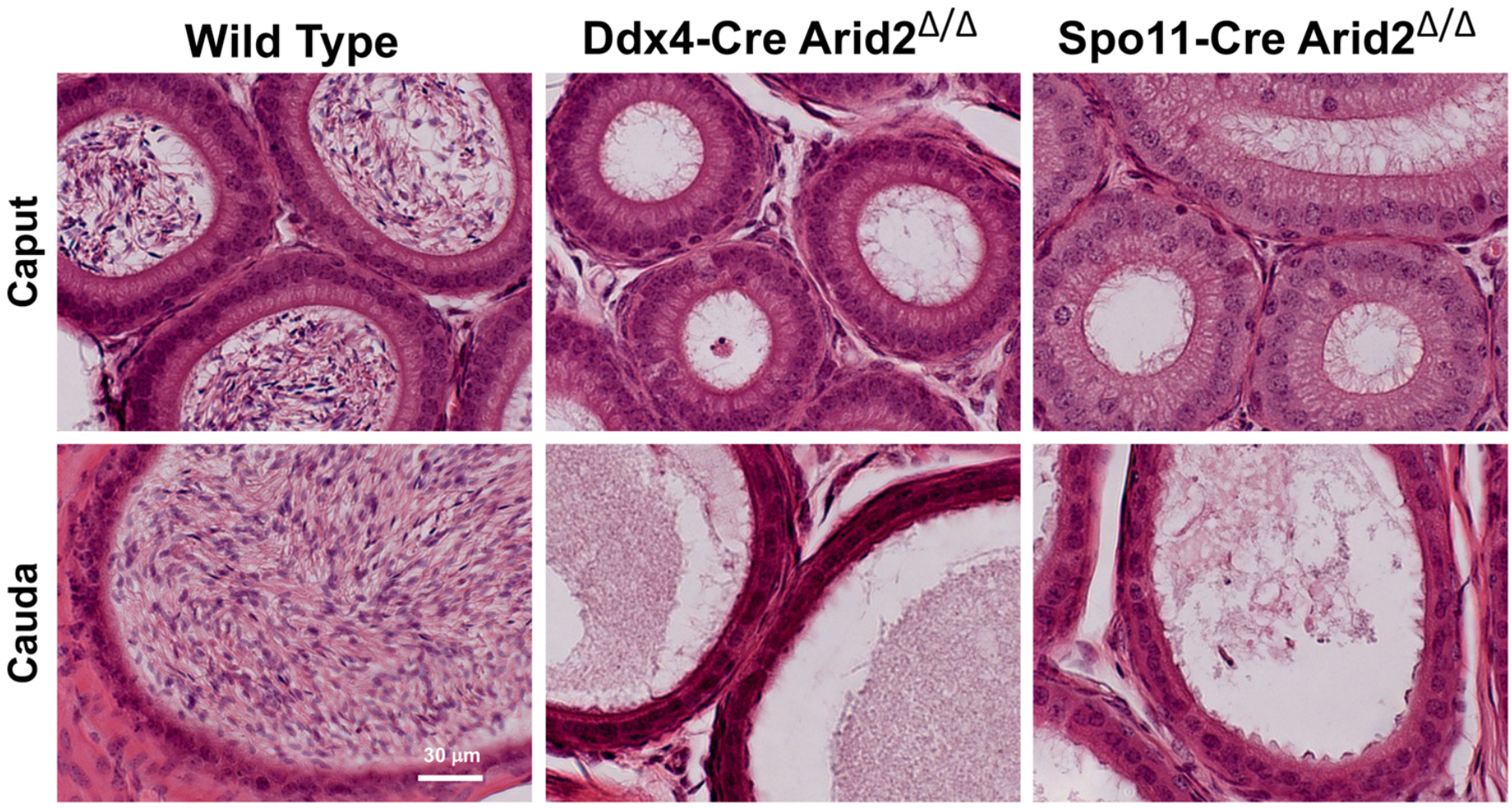

Fig. S4. Images corresponding to H&E stained epididymis tubules. Shown are the caput and cauda sections of the epididymis. Note the absent of spermatozoa in Arid2 knockout samples.

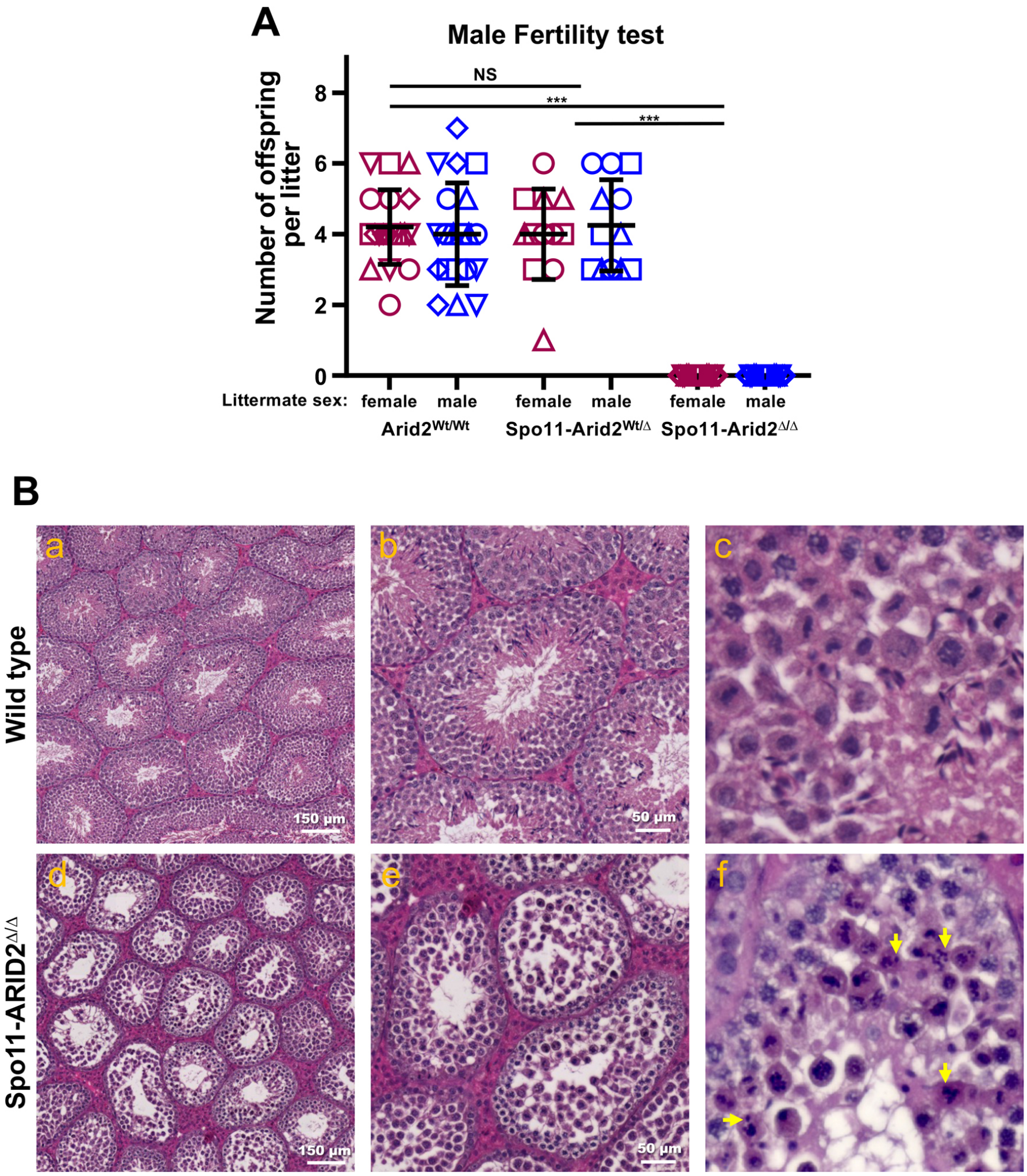

Fig. S5. Fertility assessment and testis tissue analysis of 4-months-old wild type and Arid2 knockout mice. **A.** The graph represents the number of male and female offspring resulting from mating the indicated male Arid2 genotype crossed with $Arid2^{wt/wt}$ females. NS, P=0.95. ***, P > 0.0001. Details of crosses are in Table S1. Experiments were conducted for a total of approximately 4 months. **B.** wild type and Spo11-$Arid2^{\Delta/\Delta}$ 4-months-old testis cuts stained with Hematoxylin & Eosin. Note meiosis arrest at meiosis exit in Spo11-Arid2 knockout. Arrows indicate examples of metaphase cells with lagging chromosomes.

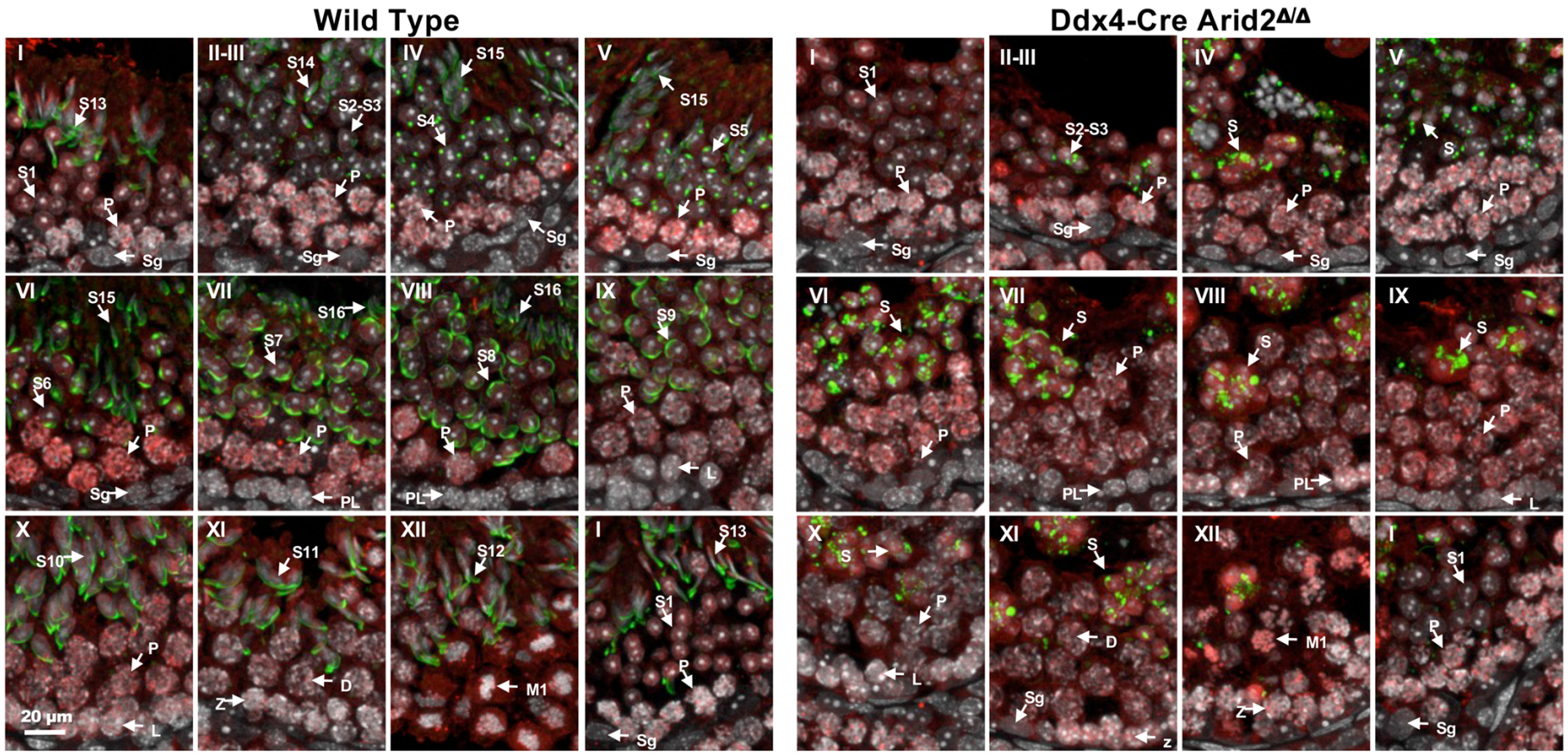

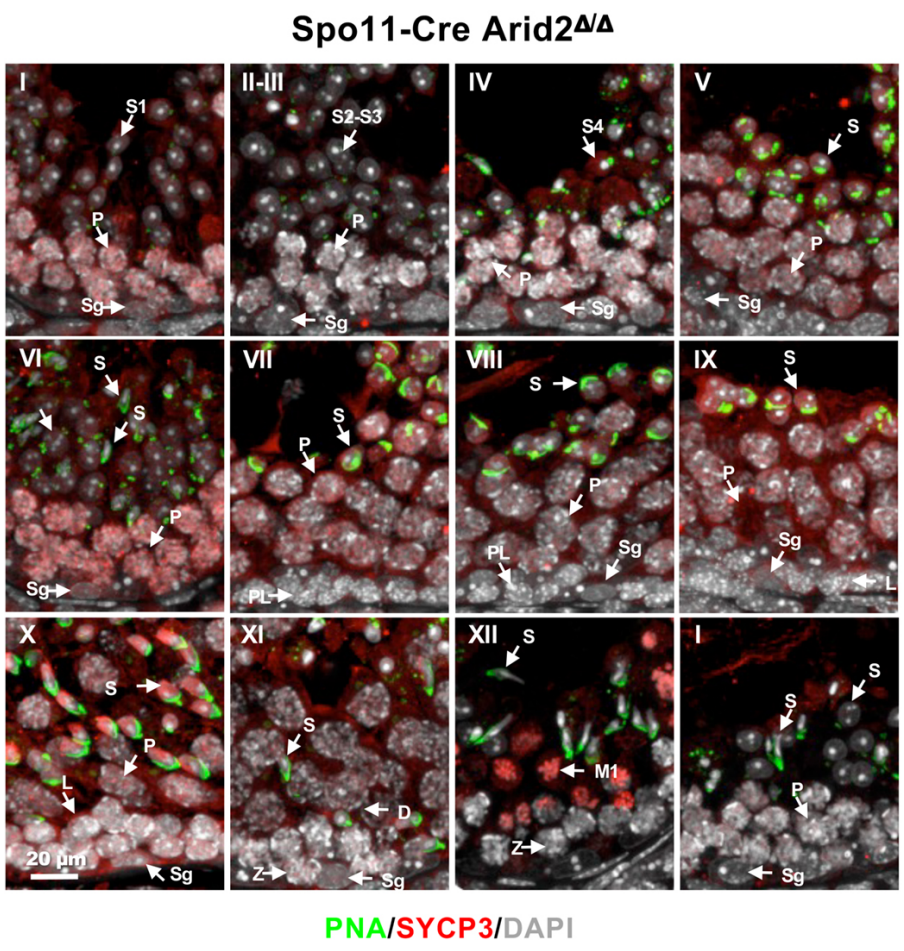

Fig. S6. Characterization of gametogenesis arrest in Arid2$^{\Delta/\Delta}$ knockout mice. Immunofluorescence of mouse seminiferous tubules with SYCP3 and lectin PNA showing representative stages I to XII. Note the spermatids differentiation failure in Ddx4-Arid2$^{\Delta/\Delta}$ and Spo11-Arid2$^{\Delta/\Delta}$ mice when compared to wild type. Sg-spermatogonia; PL-preleptotene; f and S-spermatids.

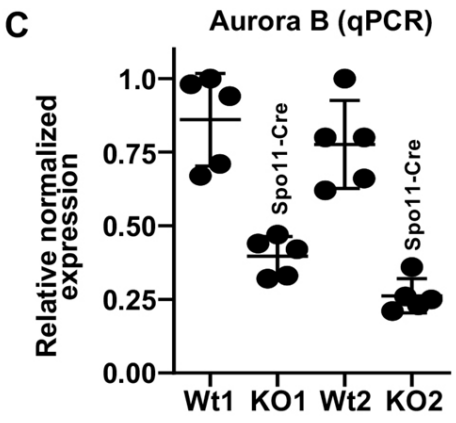

B

Strain	Aurora B	α-Tubulin	KO:WT ratio
Wt (1)	3676	11083	-
Spo11-Arid2$^{\Delta/\Delta}$ (2)	9623	13444	3.18
Wt (3)	5626	12510	-
Spo11-Arid2$^{\Delta/\Delta}$ (4)	11763	13595	2.27
Wt (5)	4307	12063	-
Spo11-Arid2$^{\Delta/\Delta}$ (6)	9525	11633	2.13
Wt (7)	11296	21878	-
Ddx4-Arid2$^{\Delta/\Delta}$ (8)	32046	17572	2.28

D

Strain	Aurora B	α-Tubulin	KO:WT ratio
Wt	4104	16227	-
Ddx4-Arid2$^{\Delta/\Delta}$	15621	14614	3.43
Wt	982	9127	-
Spo11-Arid2$^{\Delta/\Delta}$	1687	10832	2.04

Fig. S7. Aurora B expression analysis in 2-months-old wild type and Arid2 knockout testis. A. Western blot showing increase in Aurora B in three different Spo11-Arid2$^{\Delta/\Delta}$ mice compared to wild type controls. Note that the tubulin panel is same as in figure S3A. **B.** Quantitation corresponding to Aurora B and tubulin band density in western blots shown in A. o` determine Aurora B expression changes, Aurora B immunosignal intensity was normalized to the corresponding tubulin values, followed by KO/Wt ratio calculation. **C** he` graph shows values obtained from q-PCR assessment of Aurora B gene expression monitored using two independent exon boundaries in .. month-old wild type and Spo11-Arid2 knockouts. **D.** Quantitation corresponding to band density in western blots shown in figure 5A. Aurora B expression changes were calculated as described in B.

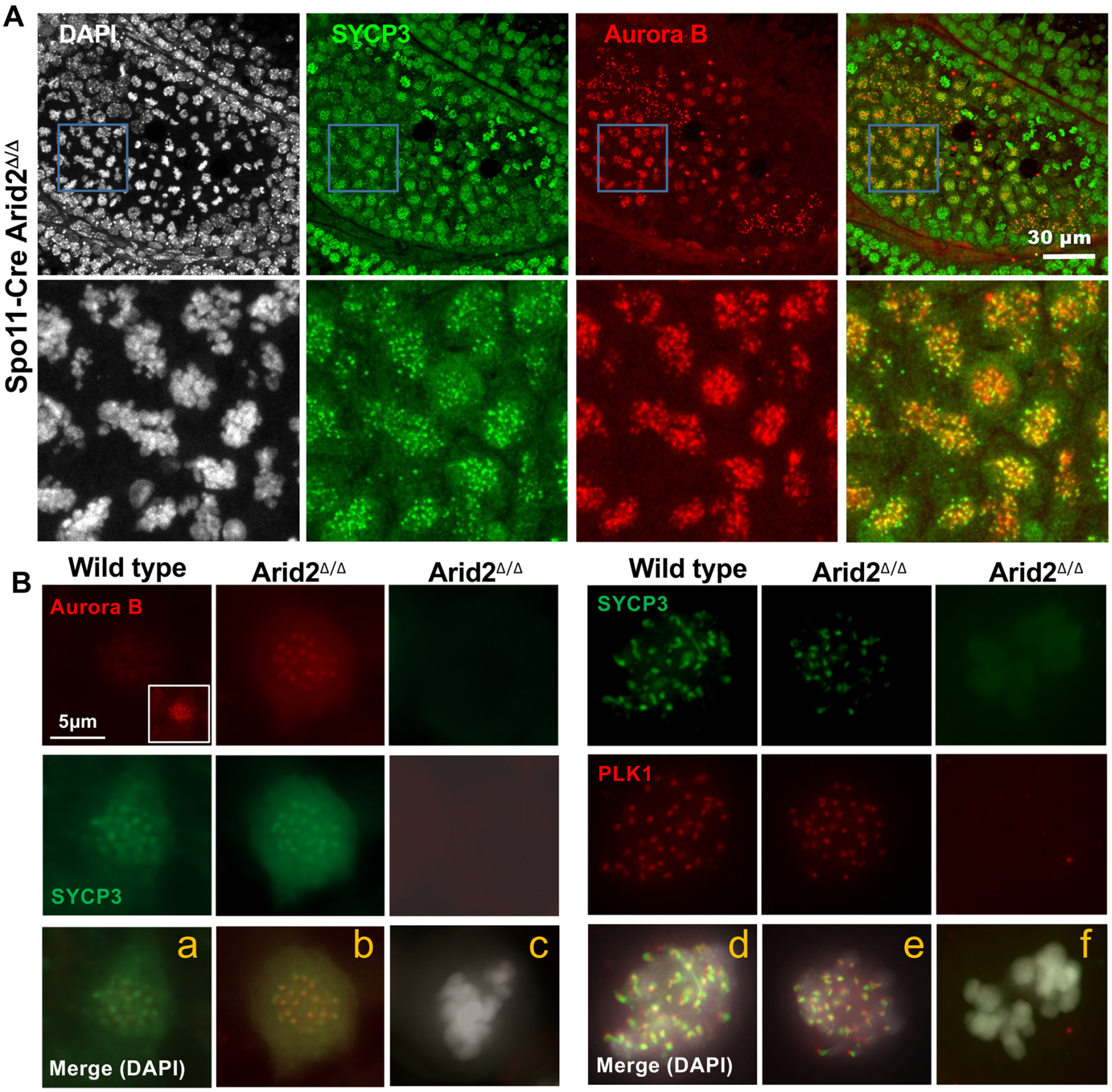

Fig. S8. A. Representative images of paraffin embedded testis cuts immunostained with SYCP3 and Aurora B in 2-month-old Spo11-Arid2 knockout mice (wild type control is shown in figure 5C top panel). The magnification (within the blue frame) shows cells transitioning metaphase-anaphase I immunostained with SYCP3 (which at this stage marks centromeres) and Aurora B. **B.** Representative images of cells at metaphase- anaphase I obtained from squashed seminiferous tubules immunostained with SYCP3, Aurora B, or PLK1 in wild type and Ddx4-Arid2 knockout mice. Note that the insert shows the cell with a longer exposure for Aurora B to allow comparison to knockout. **C.** Seminiferous tubule of 2-month-old Ddx4-Arid2$^{\Delta/\Delta}$ mice showing that PLK1 negative cells are also positive for TUNEL (marking apoptotic cells). Arrowheads indicate cells with PLK1 positive signal and negative for TUNEL. Arrows indicate cells positive for TUNEL and showing no signal for PLK1.

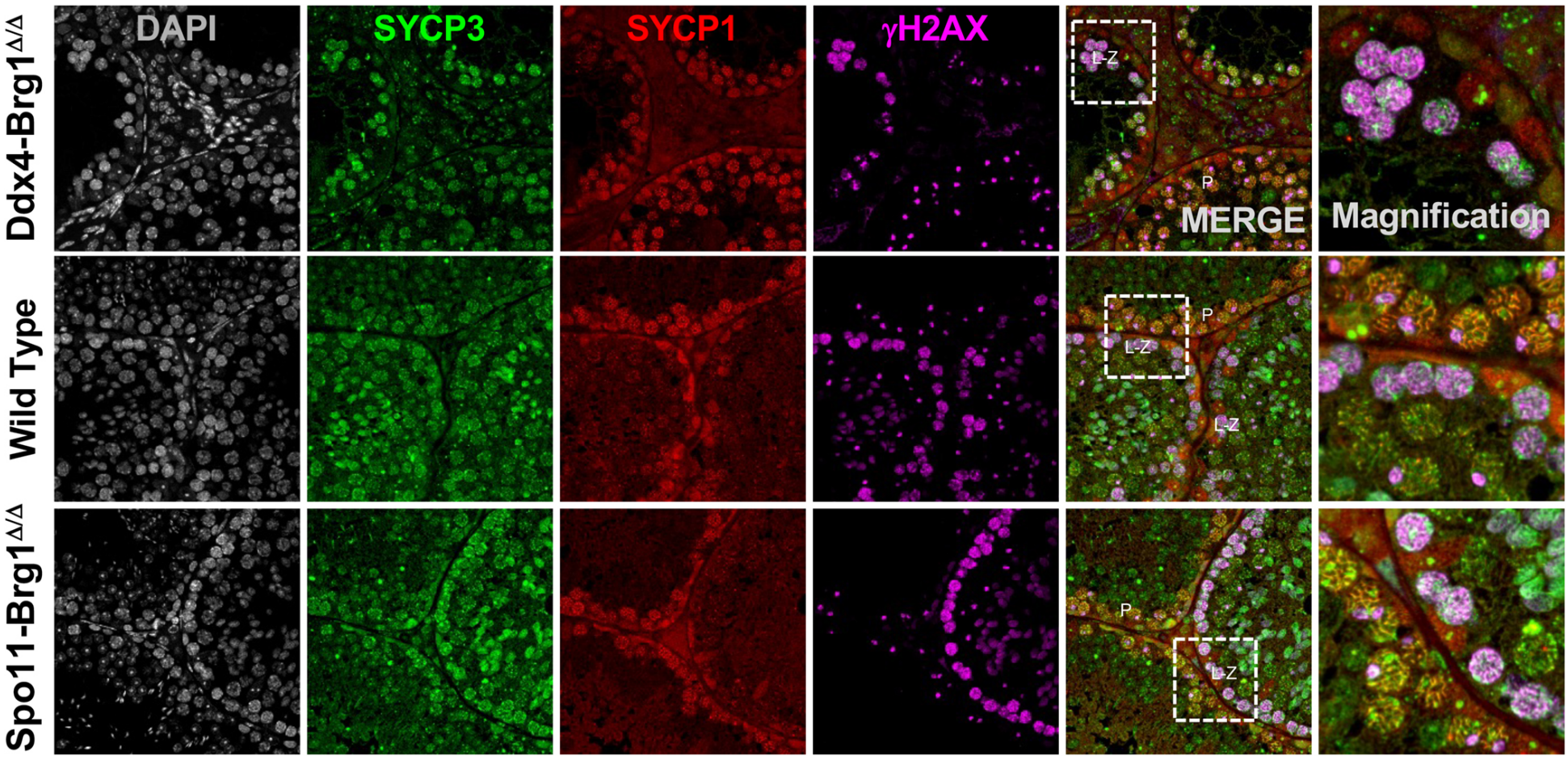

Fig. S9. Immunohistochemical analysis of 2-months-old testis cuts from Ddx4-Brg1 knockout, Spo11-Brg1 knockout, and wild type mice. Testis cuts were immunostained with SYCP1, SYCP3 and γH2AX. Magnifications in the far-right panels correspond to the white square inserts. L-Z, leptotene/zygotene and P-pachytene

Table S1. Fertility assay of wild type, heterozygous, and Spo11-Arid2 knockout mice.

Primer sequences

Primer name	Sequence (5' → 3')
ARID2 forward	GAAACTCAAACAGGGCACAAAG
ARID2 reverse	AACAGCTGCTCTCTGTGTAAG
ARID2 Δ reverse	TTGGCCTTTCAGGATAGACTTAC
LacZ forward	ATCACGACGCGCTGTATC
LacZ reverse	ACATCGGGCAAATAATATCG
BRG1 forward	GTCATACTTATGTCATAGCC
BRG1 reverse	GCCTTGTCTCAAACTGATAAG
BRG1 Δ allele forward	GATCAGCTCATGCCCTAAGG
Ddx4-Cre forward	CACGTGCAGCCGTTTAAGCCGCGT
Ddx4-Cre reverse	TTCCCATTCTAAACAACACCCTGAA
Spo11-Cre forward	CCATCTGCCACCAGCCAG
Spo11-Cre reverse	TCGCCATCTTCCAGCAGG

Table S2. Sequence of primers and PCR products for mouse genotyping.

PCRs primer pairs and expected size bands

PCR type	Forward primer	Reverse primer	Expected size band (bp)
ARID2 Wt/floxed alleles	ARID2 forward	ARID2 reverse	506 (floxed allele) 288 (Wt allele)
ARID2 Δ allele	ARID2 forward	ARID2 Δ reverse	452
LacZ Cassette	LacZ forward	LacZ reverse	108
BRG1 Wt/floxed alleles	BRG1 forward	BRG1 reverse	387 (floxed allele) 241 (Wt allele)
BRG1 Δ allele	BRG1 Δ allele forward	BRG1 reverse	268
Ddx4-Cre	Ddx4-Cre forward	Ddx4-Cre reverse	240
Spo11-Cre	Spo11-Cre forward	Spo11-Cre reverse	281

Table S3. List of antibodies and dilutions used in this study.

Antibody	Source	Western blot dilution	Immuno-labeling dilution
ARID2/BAF200	Sigma, #SAB2702507	1:2500	1:200
ARID2/BAF200	Our lab: ref: J Biol Chem. 2017 May 19; 292(20): 8459–8471. PMC5437250	1:3000	
AurkB/AIM-1	BD Biosciences, 611082	1:500	1:50
BRG1	AbCam, 110641	1:3000	
BRG1	Proteintech, 21634-1-AP		1:200
PLK1	AbCam, 17056	1:1500	1:200
PBRM1/BAF180	Bethyl, A301-591A	1:3000	
SMARCB1/BAF47	Cell Signaling Tech., #91735	1:3000	
SMARCC1/BAF155	Cell Signaling Tech., #11956	1:500	
SMARCC2/BAF170	Cell Signaling Tech., #12760	1:1000	
Survivin	NOVUS Biologicals, NB500-201	1:1000	
SMARCE1/BAF57	Cell Signaling Tech., #33360	1:1000	
SYCP3	Our lab: ref: PLoS Genet. 2018 May 9;14(5):e1007381. PMC5962103		1:300
SYCP3	AbCam, ab97672	1:1000	
SYCP1	Novus, NB300-229		1:300
γH2AX	Millipore, 05-636		1:1000
Lamin B	AbCam, 16048	1:2500	
α-tubulin	Proteintech, 66031-1-Ig	1:5000	
Lectin PNA-Alexa488	Invitrogen L21409		1:200